Seismic velocity and attenuation structures in the top 400 km of the Earth's inner core along equatorial paths

Wen-che Yu[1] and Lianxing Wen[1]

Received 11 August 2005; revised 25 April 2006; accepted 1 May 2006; published 27 July 2006.

[1] We study seismic velocity and attenuation structures in the top 400 km of the Earth's inner core based on modeling of differential traveltimes, amplitude ratios, and waveforms of the *PKiKP-PKIKP* phases observed at the epicentral distance range of 120°–141° and the *PKPbc-PKIKP* phases observed at the distance range of 146°–160° along equatorial paths. Our data are selected from the seismograms recorded in the Global Seismographic Network from 1990 to 2001 and many regional seismic networks. The observed *PKiKP-PKIKP* and *PKPbc-PKIKP* phases exhibit distinctive "east-west" hemispheric patterns: (1) At the distance ranges of 131°–141° and 146°–151°, *PKIKP* phases arrive about 0.3 s earlier than the theoretical arrivals based on the Preliminary Reference Earth Model (PREM) for the *PKIKP* phases sampling the "eastern hemisphere" (40°E–180°E) of the inner core and about 0.4 s later for those sampling the "western hemisphere" (180°W–40°E). At the distance range of 151°–160°, *PKIKP* phases arrive about 0.7 s earlier than the predicted arrivals based on PREM for those sampling the eastern hemisphere and about 0.1 s later for those sampling the western hemisphere. (2) Amplitude ratios of the *PKIKP*/*PKiKP* phases at the distance range of 131°–141° and of the *PKIKP*/*PKPbc* phases at the distance range of 146°–151° are, in general, smaller for the *PKIKP* phases sampling the eastern hemisphere than for those sampling the western hemisphere. At distances greater than 151°, the *PKIKP*/*PKPbc* amplitude ratios become indistinguishable for the two hemispheres. These observations can be best explained by two different types of seismic velocity and attenuation models along equatorial paths, one for each hemisphere, in the top 400 km of the inner core. For the eastern hemisphere, the velocity structure has a velocity increase of 0.748 km/s across the inner core boundary (ICB), a small velocity gradient of 0.0042 (km/s)/100 km in the top 235 km, followed by a steeper velocity gradient of 0.1 (km/s)/100 km extending from 235 km to 375 km, and a velocity gradient of 0.01 (km/s)/100 km in the deeper portion of the inner core; the attenuation structure has an average Q value of 300 in the top 300 km and an average Q value of 600 in the deeper portion of the inner core. For the western hemisphere, the velocity structure has a velocity increase of 0.645 km/s across the ICB and a velocity gradient of 0.049 (km/s)/100 km in the top 375 km; the attenuation structure has an average Q value of 600 in the top 375 km of the inner core. Our results suggest that the inner core hemispheric variations in velocity extend deeper than 375 km below the ICB and the top 235 km of the inner core in the eastern hemisphere is anomalous compared to the rest of the inner core in having a small velocity gradient, high velocity, and high attenuation.

Citation: Yu, W., and L. Wen (2006), Seismic velocity and attenuation structures in the top 400 km of the Earth's inner core along equatorial paths, *J. Geophys. Res.*, *111*, B07308, doi:10.1029/2005JB003995.

1. Introduction

[2] The seismic properties of the Earth's inner core exhibit complex patterns. They are constrained by two types of seismic observations: body wave and normal mode data. Body waves, mostly the *PKIKP* (*PKPdf*) phases, are sensitive to the *P* wave velocity and attenuation structures of the inner core. Since *Poupinet et al.* [1983] first observed the polar *PKIKP* traveltime anomaly, the body wave studies have revealed various remarkable features of the Earth's inner core: a magnitude of about 1–3% of velocity anisotropy with the fast direction parallel to the Earth's rotation axis [*Morelli et al.*, 1986; *Creager*, 1992; *Song and Helmberger*, 1993; *Vinnik et al.*, 1994; *Song*, 1996; *McSweeney et al.*, 1997; *Sun and Song*, 2002], the presence of a top

[1]Department of Geosciences, State University of New York at Stony Brook, Stony Brook, New York, USA.

0148-0227/06/2005JB003995$09.00

isotropic layer overlying deep anisotropy [*Shearer*, 1994; *Song and Helmberger*, 1995a, 1998; *Garcia and Souriau*, 2000; *Niu and Wen*, 2001; *Ouzounis and Creager*, 2001; *Niu and Wen*, 2002] and a change of velocity anisotropy near the center of the inner core [*Ishii and Dziewonski*, 2002]. Inner core anisotropy also exhibits lateral variations from a hemispheric scale [*Tanaka and Hamaguchi*, 1997; *Creager*, 1999; *Garcia and Souriau*, 2000; *Ouzounis and Creager*, 2001; *Niu and Wen*, 2002] to a regional scale [*Creager*, 1997; *Song*, 2000]. Temporal variations of *PKIKP* traveltimes are also observed and are interpreted as caused by a differential motion of the inner core [*Song and Richards*, 1996; *Creager*, 1997; *Song*, 2000; *Song and Li*, 2000; *Li and Richards*, 2003; *Zhang et al.*, 2005]. In addition to the anisotropic structure, seismic velocity structure along equatorial paths exhibits regional variations varying in different scales [*Cormier and Choy*, 1986; *Kaneshima*, 1996; *Vidale and Earle*, 2000; *Niu and Wen*, 2001; *Wen and Niu*, 2002; *Stroujkova and Cormier*, 2004; *Koper et al.*, 2004]. The studies of the amplitudes and waveforms of the *PKIKP* phases also suggested complex features of the attenuation structure in the inner core, including its frequency dependence [*Doornbos*, 1983; *Cormier et al.*, 1998; *Li and Cormier*, 2002], depth dependence [*Doornbos*, 1974; *Cormier*, 1981; *Souriau and Roudil*, 1995; *Song and Helmberger*, 1995b; *Tseng et al.*, 2001; *Li and Cormier*, 2002; *Cormier and Li*, 2002], direction dependence [*Souriau and Romanowicz*, 1996, 1997; *Cormier et al.*, 1998; *Oreshin and Vinnik*, 2004] and lateral variations [*Tseng et al.*, 2001; *Wen and Niu*, 2002; *Li and Cormier*, 2002; *Oreshin and Vinnik*, 2004; *Cao and Romanowicz*, 2004a]. A recent study observed a ubiquitous correlation of high velocity with high attenuation, and suggested that the velocity attenuation correlation can be explained by attenuation anisotropy in the inner core [*Yu and Wen*, 2006]. In addition, precritical *PKiKP* amplitudes have been used to investigate the density contrast and the sharpness of the inner core boundary [*Cummins and Johnson*, 1988; *Souriau and Souriau*, 1989; *Cao and Romanowicz*, 2004b; *Krasnoshchekov et al.*, 2005].

[3] The split of the normal modes of the Earth's free oscillation provides another powerful probe to study the elastic properties and density of the inner core. Anisotropy, large-scale density and velocity anomalies, or structures departed from the spherical symmetry such as the Earth's rotation or ellipticity of the Earth's boundaries, would cause the singlet eigenfrequency to split. Anomalous splitting of the modes that are sensitive to the inner core structures was first identified by *Masters and Gilbert* [1981]. Subsequent studies of the normal modes indicated that the inner core anisotropy is a preferred explanation for the anomalous splitting of those modes [*Woodhouse et al.*, 1986; *Tromp*, 1993, 1995; *Durek and Romanowicz*, 1999; *Ishii et al.*, 2002]. Anomalous splitting of the core sensitive modes has also been used to investigate the differential motion of the inner core [*Laske and Masters*, 1999] and the depth dependence of the anisotropy [*Durek and Romanowicz*, 1999; *Beghein and Trampert*, 2003].

[4] Recent seismic studies revealed "east-west" hemispheric variations in seismic isotropic velocity and attenuation in the uppermost 80 km of the Earth's inner core [*Niu and Wen*, 2001; *Wen and Niu*, 2002; *Garcia*, 2002; *Stroujkova and Cormier*, 2004; *Cao and Romanowicz*, 2004a]. These studies indicated that the top portion of the inner core beneath the eastern hemisphere (40°E–180°E) has higher velocities (about 0.8–1.3% faster), a smaller velocity gradient, and higher attenuation than the western hemisphere (180°W–40°E) [*Niu and Wen*, 2001; *Wen and Niu*, 2002; *Garcia*, 2002; *Stroujkova and Cormier*, 2004; *Cao and Romanowicz*, 2004a]. It is interesting to note that the velocity anisotropy observed in the deeper part of the inner core also exhibits a similar hemispheric pattern, with a large magnitude of anisotropy in the western hemisphere and a weak anisotropy in the eastern hemisphere [*Tanaka and Hamaguchi*, 1997; *Song and Helmberger*, 1998; *Creager*, 1999; *Garcia and Souriau*, 2000; *Ouzounis and Creager*, 2001; *Niu and Wen*, 2002]. It becomes important to establish one-dimensional seismic velocity and attenuation structures along equatorial paths (defined as the *PKIKP* ray angles are greater than 35° from the Earth's rotation axis) in the top 400 km of the inner core for the two hemispheres for several reasons: (1) it remains unclear how deep the hemispheric variations in velocity and attenuation in the top portion of the inner core extend in the inner core; (2) seismic structures along equatorial paths serve as the baseline for understanding the magnitude of seismic anisotropy and the level of seismic heterogeneity; (3) seismic structures in the deeper portion of the inner core strongly depend on the inferred seismic structures in the top portion of the inner core, as the seismic waves sampling the deeper portion unavoidably propagate through the top portion of the inner core [*Wen and Niu*, 2002]; and (4) these inferred seismic structures would place fundamental constraints on the composition, geodynamics, and mineral physics of the inner core.

[5] In this paper, we establish seismic velocity and attenuation structures along equatorial paths in the top 400 km of the inner core for the eastern and western hemispheres, by studying the differential traveltimes, amplitude ratios, and waveforms of two core phase pairs sampling along equatorial paths. We discuss seismic data and coverage in section 2, detailed observations and seismic

Figure 1. (a) Ray paths of three *PKP* branches based on the Preliminary Reference Earth Model (PREM) [*Dziewonski and Anderson*, 1981]. *PKIKP*, *PKiKP* at an epicentral distance of 141°, and *PKIKP*, *PKPbc* at 147°. (b, c) Map view of great circle paths (gray lines) and ray segments of the *PKIKP* phases sampling the inner core (black lines) recorded by the Global Seismographic Network (GSN) (Figure 1b) and several regional seismic networks: Grafenberg (GRF), the German Regional Seismic Network (GRSN), GEOSCOPE, GEOFON, the Broadband Andean Joint Experiment (BANJO), the Brazilian Lithosphere Seismic Project (BLSP), the Seismic Exploration Deep Andes (SEDA), FREESIA, along with the GSN stations in Europe (Figure 1c). Stars and triangles represent locations of earthquakes and seismic stations, respectively. The geographic region of the two hemispheres is marked, with the eastern hemisphere defined between 40°E–180°E and the western hemisphere defined between 180°W–40°E.

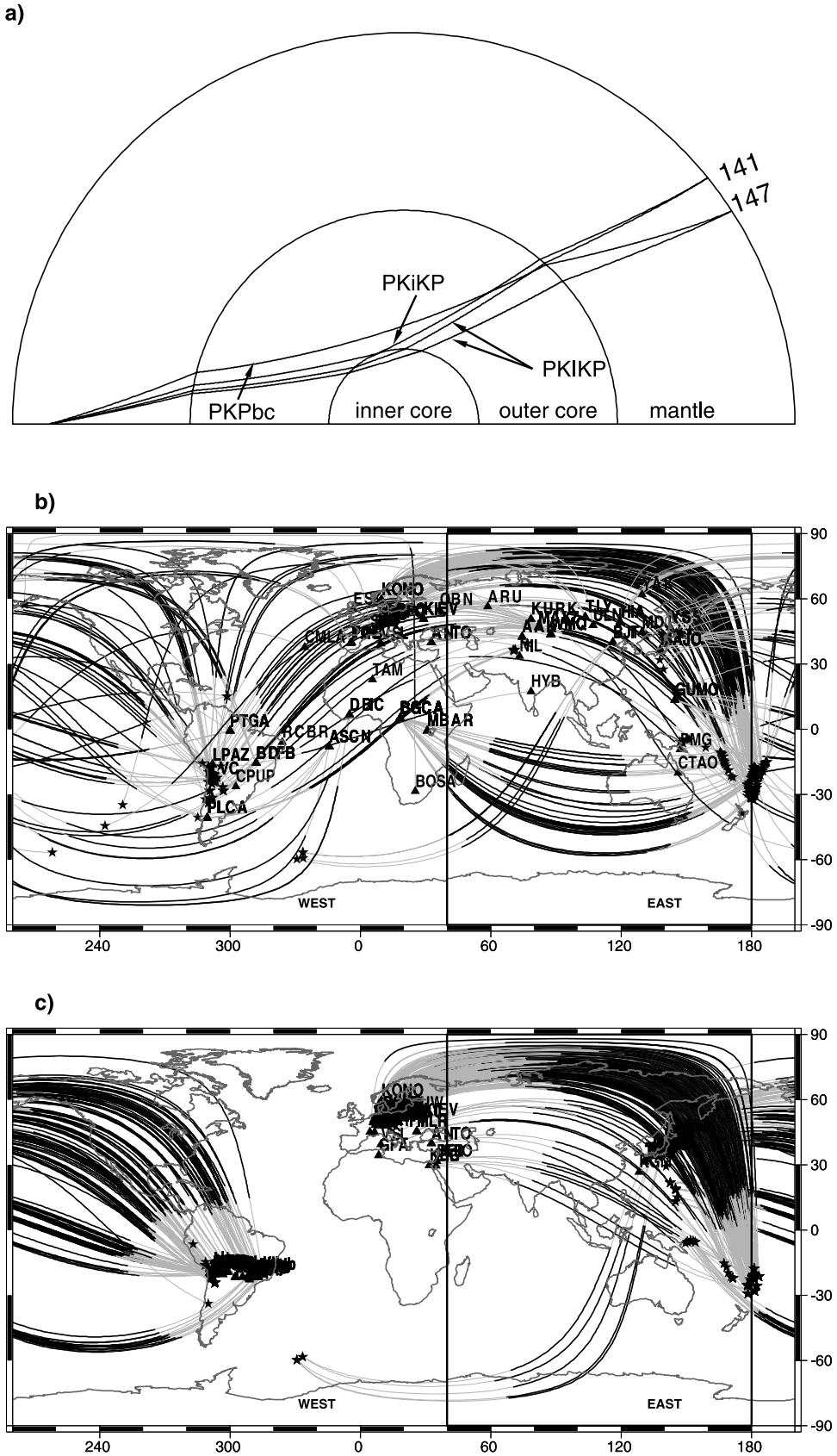
a)
141
147
PKiKP
PKIKP
PKPbc
inner core
outer core
mantle
b)
KONO
ESK
OBN
ARU
KIEV
ANTO
NIL
TAM
HYB
DBIC
BGCA
MBAR
PTGA
RCBR
ASCN
LPAZ
BDFB
CPUP
PLCA
BOSA
GUMO
PMG
CTAO
WEST
EAST
90
60
30
0
-30
-60
-90
240
300
0
60
120
180
c)
KONO
KIEV
ANTO
CPA
WEST
EAST
90
60
30
0
-30
-60
-90
240
300
0
60
120
180

Figure 1

Table 1. Event List[a]

Event	Origin Date	Origin Time, UT	Latitude, °N	Longitude, °E	Depth, km
19900220	1990/02/20	1817:00	−21.54	170.47	159
19900322	1990/03/22	0211:50	−8.42	158.88	115
19900508	1990/05/08	0140:00	−17.01	168.45	226
19900517	1990/05/17	1103:00	−18.17	−69.82	109
19900728	1990/07/28	0842:00	−15.32	167.35	111
19901104	1990/11/04	1813:42	−15.70	−72.70	114
19920416	1992/04/16	1833:00	−20.11	−68.53	122
19920528	1992/05/28	0927:12	−30.42	−178.14	60
19930110	1993/01/10	1439:03	−59.37	−26.29	84
19930209	1993/02/09	1425:38	45.69	141.93	306
19930224	1993/02/24	2221:37	−24.90	−68.38	117
19930502	1993/05/02	1526:03	−21.11	−175.88	123
19930530	1993/05/30	1632:28	−5.48	150.49	110
19930608	1993/06/08	2317:41	−31.59	−69.22	113
19930826	1993/08/26	0332:42	−5.49	154.21	135
19930929	1993/09/29	1903:07	−6.07	149.49	63
19931008	1993/10/08	1823:46	46.49	150.02	163
19931011	1993/10/11	1554:00	32.00	137.85	365
19931019	1993/10/19	0402:22	−22.39	−66.00	278
19931110	1993/11/10	0003:25	−4.68	151.91	113
19940506	1994/05/06	2239:29	−4.74	153.10	78
19940813	1994/08/13	2207:09	15.13	145.87	87
19940822	1994/08/22	1726:38	−11.50	166.42	148
19940830	1994/08/30	0613:36	44.71	150.14	54
19940831	1994/08/31	0907:26	43.70	145.99	80
19940930	1994/09/30	1930:17	−21.06	−179.25	613
19941018	1994/10/18	1712:51	43.55	147.12	65
19941109	1994/11/09	1821:03	43.52	147.19	60
19941124	1994/11/24	1321:15	−5.33	150.49	142
19941218	1994/12/18	2038:33	−17.86	−178.69	551
19941230	1994/12/30	1512:26	18.59	145.27	234
19950115	1995/01/15	2359:26	−5.26	152.03	66
19950120	1995/01/20	0335:46	43.26	146.82	60
19950121	1995/01/21	0847:29	43.34	146.72	62
19950218	1995/02/18	1329:06	46.67	145.89	354
19950318	1995/03/18	0927:19	29.28	140.69	103
19950325	1995/03/25	2244:28	−11.05	166.11	77
19950331	1995/03/31	1401:40	38.15	135.06	364
19950408	1995/04/08	1745:18	21.80	142.63	318
19950502	1995/05/02	0354:08	43.26	147.35	50
19950518	1995/05/18	1431:14	44.32	147.58	103
19950525	1995/05/25	0459:51	43.91	147.37	76
19950623	1995/06/23	1610:56	−24.58	−177.28	108
19950707	1995/07/07	2115:18	33.95	137.12	323
19950817	1995/08/17	2314:00	36.47	71.16	239
19950818	1995/08/18	0157:18	13.21	145.15	71
19950823	1995/08/23	1314:42	−56.75	−141.68	10
19950824	1995/08/24	0155:34	18.92	144.95	588
19950824	1995/08/24	0628:54	18.88	145.01	600
19950912	1995/09/12	1423:33	−21.60	−179.43	599
19950918	1995/09/18	2022:14	−20.55	−178.68	617
19951014	1995/10/14	0800:42	−25.57	−177.51	70
19951210	1995/12/10	2347:00	−21.25	−178.11	403
19960507	1996/05/07	2320:00	43.71	147.61	54
19960526	1996/05/26	0143:44	−22.19	171.48	108
19960530	1996/05/30	0304:37	−56.72	−26.31	84
19961025	1996/10/25	1959:41	−17.38	−69.99	116
19961114	1996/11/14	1347:38	−21.24	−176.62	192
19970311	1997/03/11	0313:59	−21.13	−178.86	553
19970401	1997/04/01	1833:32	−18.30	−69.53	114
19970401	1997/04/01	1842:00	−18.35	−69.35	116
19970411	1997/04/11	0534:42	39.53	76.94	15
19970412	1997/04/12	0921:56	−28.17	−178.37	184
19970420	1997/04/20	1953:00	−34.04	−69.98	105
19970503	1997/05/03	1646:02	−31.79	−179.38	108
19970826	1997/08/26	1522:09	−25.51	178.33	610
19970928	1997/09/28	2313:13	−22.41	−68.45	107
19971005	1997/10/05	1804:30	−59.74	−29.20	274
19971008	1997/10/08	1047:49	−29.25	178.35	617
19971022	1997/10/22	0955:00	44.72	146.21	154
19980127	1998/01/27	1955:00	−22.54	179.05	611
19980325	1998/03/25	2102:55	−24.34	−66.99	197
19980414	1998/04/14	0341:22	−23.82	−179.87	499
19980901	1998/09/01	1029:49	−58.21	−26.53	152
19980912	1998/09/12	0903:48	−24.51	−67.12	187
19981008	1998/10/08	0451:42	−16.12	−71.40	136
19990205	1999/02/05	1139:00	−12.62	166.97	213
19990305	1999/03/05	0033:00	−20.42	−68.90	111
19990306	1999/03/06	2028:54	−21.73	−179.46	603
19990323	1999/03/23	1123:44	−20.91	−178.73	575
19990508	1999/05/08	1944:00	45.45	151.63	63
19990802	1999/08/02	0947:00	−12.55	167.18	251
19990918	1999/09/18	2351:30	−19.71	169.21	103
19991025	1999/10/25	2031:00	−38.70	175.80	159
19991121	1999/11/21	0351:00	−21.75	−68.78	101
19991206	1999/12/06	2312:00	57.41	−154.49	66
20000119	2000/01/19	0709:00	36.37	70.38	207
20000411	2000/04/11	0641:26	−27.94	−178.39	201
20000508	2000/05/08	2135:00	−31.32	179.84	383
20000512	2000/05/12	2310:00	35.97	70.66	108
20000614	2000/06/14	0215:26	−25.52	178.05	605
20000614	2000/06/14	0319:18	−24.03	−66.75	197
20000616	2000/06/16	0755:35	−33.88	−70.09	120
20000616	2000/06/16	2023:00	−28.88	−178.46	222
20001022	2000/10/22	2026:00	−15.23	167.70	143
20001218	2000/12/18	0119:21	−21.18	−179.12	628
20010704	2001/07/04	0706:32	−21.73	−176.71	184

[a]Events in bold are the data recorded in regional seismic networks. Origin dates are year, month, day.

models in section 3, mantle effect on the differential traveltimes and amplitude ratios in section 4, and possible interpretations in section 5. In the following, the terms "eastern hemisphere" and "western hemisphere" refer to the "eastern hemisphere of the inner core" and "western hemisphere of the inner core," respectively.

2. Seismic Data and Coverage

[6] Seismic velocity and attenuation structures along equatorial paths in the top 400 km of the Earth's inner core are constrained by modeling the differential traveltimes, amplitude ratios, and waveforms of the *PKiKP-PKIKP* phases at the epicentral distance range of 120°–141° and the *PKPbc-PKIKP* phases at the distance range of 146°–160°. *PKIKP* is the *P* wave transmitted through the inner core; *PKiKP* is the *P* wave reflected off the inner core boundary (ICB); and *PKPbc* is the *P* wave propagating through the bottom portion of the outer core (Figure 1a). Since the ray paths of these phase pairs are close in the mantle, the seismic heterogeneities in the mantle would affect the *PKIKP* and *PKiKP* (*PKPbc*) phases in a similar way (Figure 1a). The differential traveltimes and amplitude ratios of the *PKiKP-PKIKP* and *PKPbc-PKIKP* phases are thus most sensitive to the velocity and attenuation structures of the inner core. In this study, we only use the *PKiKP-PKIKP* phases observed at the distance range of 120°–141° and the *PKPbc-PKIKP* phases recorded at the distance range of 146°–160°. The seismic data at these two distance ranges are sensitive to the seismic structures in the top 80 km and 140–400 km of the inner core, respectively. At the distance range of 141°–146° (corresponding to the *PKIKP* turning depth of 80–140 km in the inner core), *PKIKP* and *PKiKP* phases are interfered with the long-period *PKPB*diff, a *P* wave transmitted in the middle portion of the outer core,

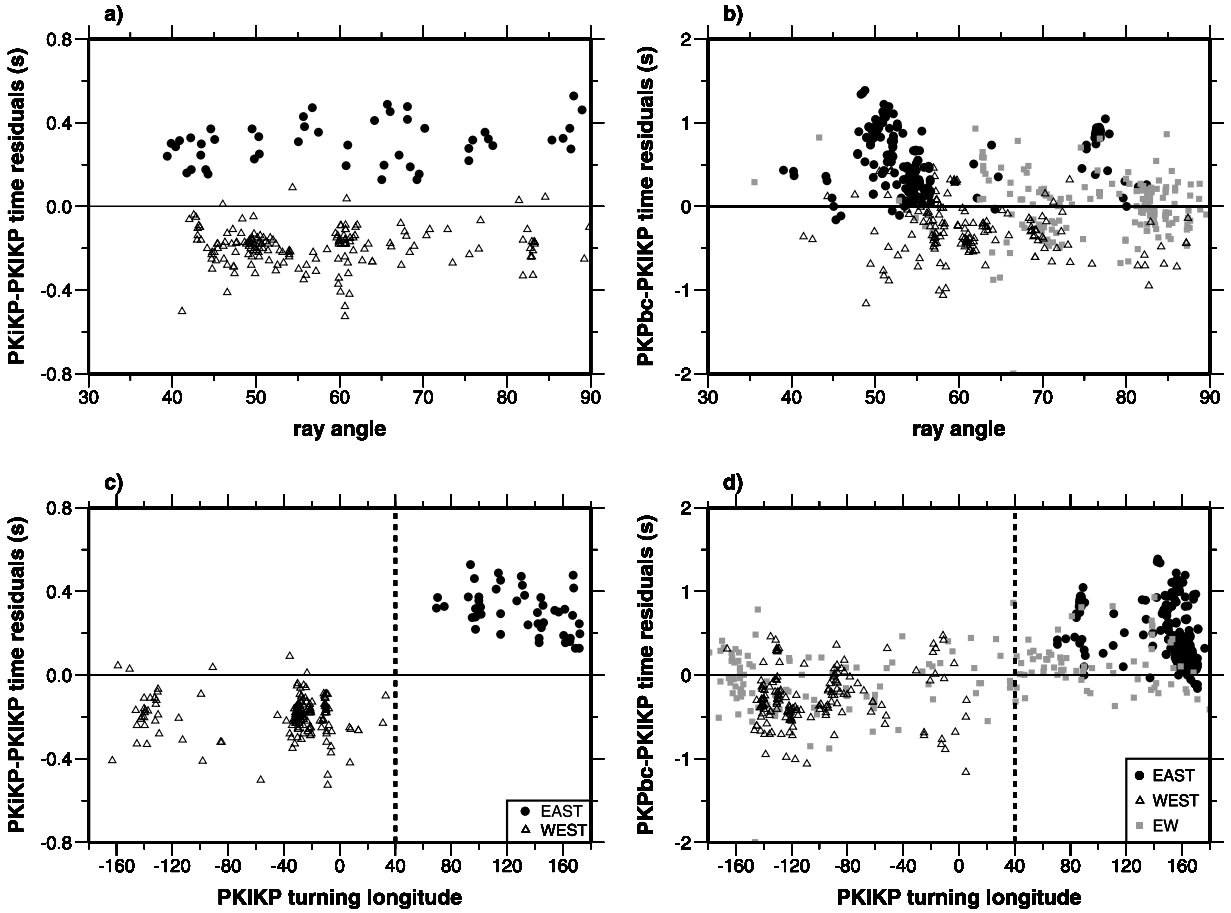

Figure 2. Observed *PKiKP-PKIKP* and *PKPbc-PKIKP* differential traveltime residuals with respect to PREM as a function of (a, b) ray angle and (c, d) *PKIKP* turning longitude. The meaning of the symbols is shown in the inset. Solid circles (labeled as EAST) are the observations for the *PKIKP* ray segments in the inner core confined in the eastern hemisphere; open triangles (labeled as west) are the observations for the *PKIKP* ray segments in the inner core confined in the western hemisphere. Gray squares (labeled as EW) in Figures 2b and 2d are the observations that the *PKIKP* ray segments in the inner core sample across the eastern and western hemispheres. The differential traveltime residuals do not exhibit any direction dependence for the ray angles (*PKIKP* ray directions in the inner core relative to the Earth's rotation axis) being greater than 35° (Figures 2a and 2b). Note that the *PKPbc-PKIKP* differential traveltime residuals for the EW group lie between those for the eastern (east group) and western (west group) hemispheres (Figures 2b and 2d).

making the measurement of the differential traveltimes of the *PKiKP-PKIKP* phases difficult. Joint analyses of the *PKiKP-PKIKP* phases and *PKPbc-PKIKP* phases, however, can constrain the seismic structures in the top 80 km of the inner core and at depths larger than 140 km below the ICB.

[7] Broadband *PKP* seismograms are collected from the recordings in the Global Seismographic Network (GSN) of the Incorporated Research Institutions for Seismology (IRIS) Consortium from 1990–2001 and in many regional seismic networks: Grafenberg (GRF), the German Regional Seismic Network (GRSN), GEOFON, GEOSCOPE, MEDNET, the Czech Regional Seismological Network (CRSN), the Broadband Andean Joint Experiment (BANJO), the Seismic Exploration of Deep Andes (SEDA), the Brazilian Lithosphere Seismic Project (BLSP), the Kazakhstan, and the FREESIA. Part of the observations are the collections from previous studies used for studying the seismic structures in the top 80 km of the inner core [*Niu and Wen*, 2001; *Wen and Niu*, 2002; *Niu and Wen*, 2002] and in the bottom of the outer core [*Yu et al.*, 2005]. Broadband seismograms are band-pass filtered with the World-Wide Standard Seismograph Network (WWSSN) short-period instrument response. We select the data based on the simplicity of the earthquake source and high signal-to-noise ratio (see Table 1 and Table 1 of *Yu et al.* [2005] for the earthquake parameters). A total of 260 *PKiKP-PKIKP* and 830 *PKPbc-PKIKP* high-quality observations are selected based on the above criteria from a collection of more than 16,000 seismograms. Our selected data exhibit good global coverage (Figures 1b and 1c). The amplitude ratios and differential traveltimes are measured based on the ratios and the time separations between the maximum amplitudes of these phase pairs, respectively. The traveltime measurement is proved to be comparable to that determined from the waveform cross correlation and the difference in traveltime measurement between the two methods is less than 0.05 s. The differential

traveltime residuals are obtained from subtracting the predicted differential traveltimes based on the reference model PREM [*Dziewonski and Anderson*, 1981] from the observations. The observed amplitude ratios are corrected for the radiation patterns of the earthquake sources, although the effect is very small due to the similar takeoff angles of these phase pairs.

[8] Since our goal is to derive seismic velocity and attenuation structures along equatorial paths for both the eastern and western hemispheres, we only analyze the data

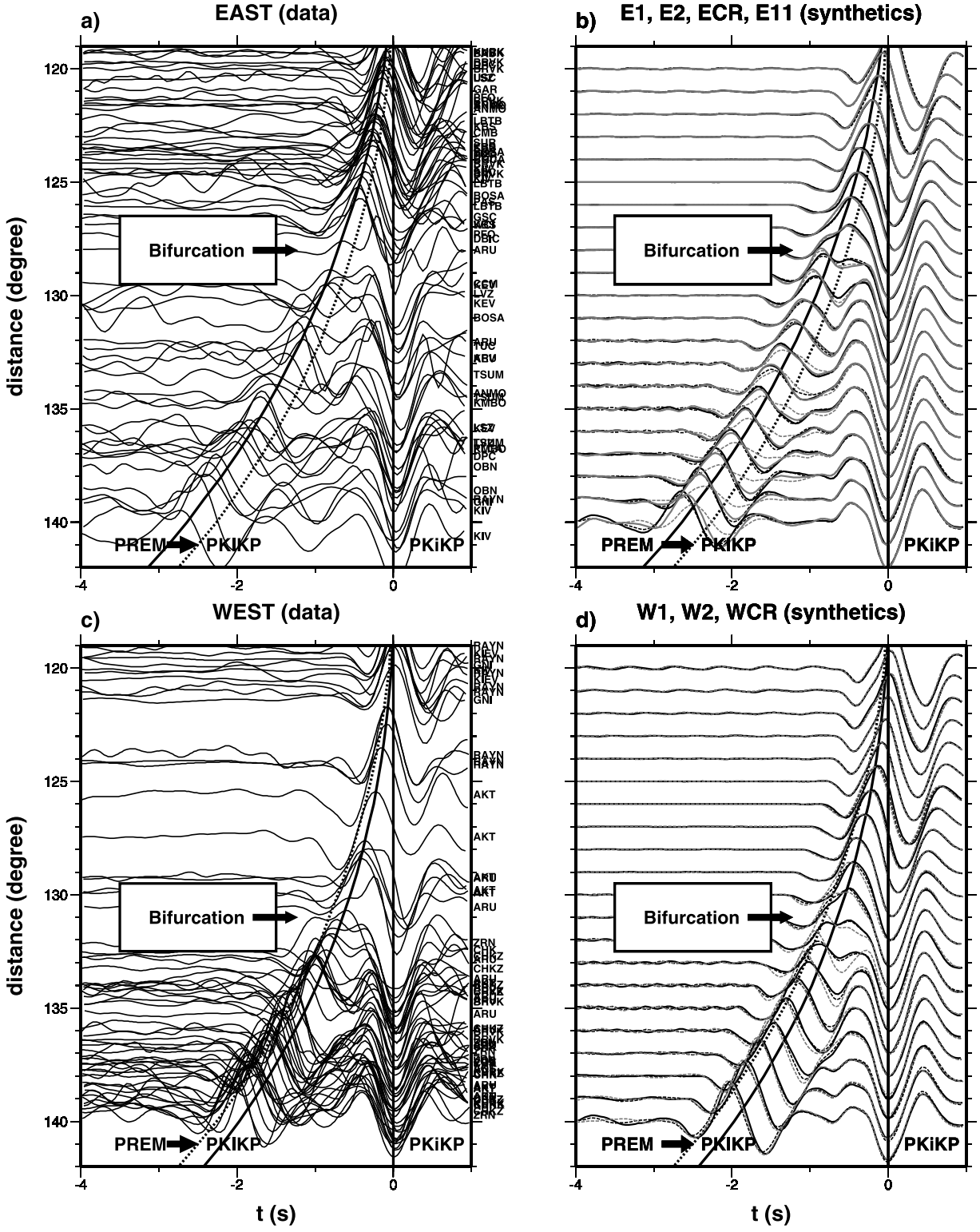

Figure 3

with the *PKIKP* ray segments confined in each of the hemispheres of the inner core and sampling along the equatorial direction. The differential traveltimes of both the *PKiKP-PKIKP* and *PKPbc-PKIKP* phases do not exhibit any direction dependence within the equatorial group (Figures 2a and 2b), indicating that the influence of inner core anisotropy is little for the data sampling along the equatorial paths we defined. The east-west hemispheric boundary at 40°E and 180°E longitudes is primarily determined by the geographic distribution of the sampling of the *PKiKP-PKIKP* differential traveltimes [e.g., *Niu and Wen*, 2001, Figure 1]. We have not specifically searched for the *PKiKP-PKIKP* data sampling the region near 40°E and 180°E longitudes to address the exact east-west hemispheric geographic boundary (Figure 2c), but our *PKPbc-PKIKP* data provide additional sampling of the east-west lateral transition (Figure 2d). The differential *PKPbc-PKIKP* traveltimes are consistent with the division of the two hemispheres inferred from the *PKiKP-PKIKP* observations (Figure 2d).

3. Seismic Observations and Detailed Seismic Velocity and Attenuation Structures Along Equatorial Paths

3.1. Seismic Observations

[9] Differential traveltime residuals, amplitude ratios, and waveforms exhibit clear east-west hemispheric patterns for both the *PKiKP-PKIKP* and *PKPbc-PKIKP* data sets. The observed *PKiKP-PKIKP* phases show these characteristics (Figures 2c, 3a, and 3c): (1) at the distance range of 131°–141°, *PKIKP* phases arrive about 0.3 s earlier than the theoretical arrivals based on PREM for the *PKIKP* phases sampling the eastern hemisphere and about 0.4 s later for those sampling the western hemisphere; (2) the bifurcation of the *PKiKP-PKIKP* phases occurs at a closer distance for those sampling the eastern hemisphere (bifurcation refers to the beginning of the visual separation of the *PKIKP* phase from the *PKiKP* phase in the short period seismograms); and (3) *PKIKP* phases have smaller amplitudes for those sampling the eastern hemisphere [see also *Wen and Niu*, 2002, Figure 7]. The observed *PKPbc-PKIKP* phases show these characteristics (Figures 4 and 5): (1) at the distance range of 146°–151°, *PKIKP* phases arrive about 0.3 s earlier than the theoretical arrivals based on PREM for the *PKIKP* phases sampling the eastern hemisphere and about 0.4 s later for those sampling the western hemisphere; at the distance range of 151°–160°, *PKIKP* phases arrive about 0.7 s earlier than the theoretical arrivals based on PREM for the *PKIKP* phases sampling the eastern hemisphere and about 0.1 s later for those sampling the western hemisphere (Figure 4); and (2) at the distance range of 146°–151°, the observed *PKIKP*/*PKPbc* amplitude ratios are, in general, smaller for the *PKIKP* phases sampling the eastern hemisphere than for those sampling the western hemisphere; at the distance range of 151°–160°, the observed *PKIKP*/*PKPbc* amplitude ratios become indistinguishable for the two hemispheres (Figure 5). The *PKPbc-PKIKP* observations at the distance range of 146°–151° exhibit same hemispheric patterns as the *PKiKP-PKIKP* observations at the distance range of 131°–141°. The east-west hemispheric patterns are also consistently observed in the data recorded in both the global and regional networks.

3.2. Seismic Velocity Structures in the Top 400 km of the Inner Core Along Equatorial Paths for the Two Hemispheres

[10] The observed *PKiKP-PKIKP* waveforms and the *PKPbc-PKIKP* differential traveltime residuals are used to constrain the seismic velocity structures in the top 400 km of the inner core along equatorial paths. Large (small) differential traveltimes would indicate high (low) velocities in the inner core. The *PKiKP-PKIKP* and *PKPbc-PKIKP* waveforms are sensitive to the seismic structures in different parts of the inner core. Joint modeling of both data sets is required as trade-offs exist for explaining each data set. The *PKiKP-PKIKP* waveforms are sensitive to the *P* velocity increase across the ICB and the radial velocity structure in the top 80 km of the inner core. The *P* velocity increase across the ICB can be derived from fitting the bifurcation (the visual separation of the *PKIKP* phase from the *PKiKP* phase in the short-period seismograms) distance. A smaller

Figure 3. (a, c) Examples of the observed waveforms for the *PKiKP* and *PKIKP* phases sampling the eastern (Figure 3a) and western (Figure 3c) hemispheres of the inner core recorded in the GSN (a) and the GSN and the Kazakhstan Network (Figure 3c); (b, d) synthetic waveforms based on E1 (black solid traces), E2 (black dashed traces), ECR (gray dashed traces), E11 (gray solid traces) (Figure 3b), and W1 (black solid traces), W2 (black dashed traces), WCR (gray dashed traces) (Figure 3d) (see Figure 6 for the velocity and attenuation models of E1, E2, W1, W2, and Figure 7 of *Cao and Romanowicz* [2004a] for the attenuation models of ECR, WCR; E11 has increased Q values from 200 to 400 in the depth range of 32 km to 85 km of the inner core). The maximum *PKiKP* amplitudes are impossible to pick at distances less than 127° for the seismic waves sampling the eastern hemisphere (Figure 3a) and at distances less than 130° for those sampling the western hemisphere (Figure 3c), due to the interference of the *PKiKP* and *PKIKP* phases. For those distances, the synthetics are aligned along the predicted *PKiKP* amplitudes based on E1 (black solid line, Figure 3b) and W1 (black solid line, Figure 3d). Observed waveforms are aligned according to waveform fitting the synthetics (Figure 3a based on Figure 3b; Figure 3c based on Figure 3d). Because of the interference of the *PKiKP* and *PKIKP* phases, there appears an offset in aligning the later maximum amplitudes at closer distances. At larger distances, synthetic and observed waveforms are aligned along the maximum amplitudes of the *PKiKP* phases. Distance corrections are made to a source depth of 200 km. Accordingly, synthetics are calculated based on a source depth of 200 km. *PKIKP* theoretical arrivals based on PREM and E1, W1 are indicated by the dotted and solid lines, respectively. Note that the *PKiKP-PKIKP* phases sampling the western hemisphere exhibit same characteristics for the seismic data recorded in the GSN and those recorded in the regional seismic networks: the Kazakhstan Network in Asia and the BLSP, BANJO, SEDA in South America (Figure 3c, and see also Figures 3 and 5 of *Wen and Niu* [2002]).

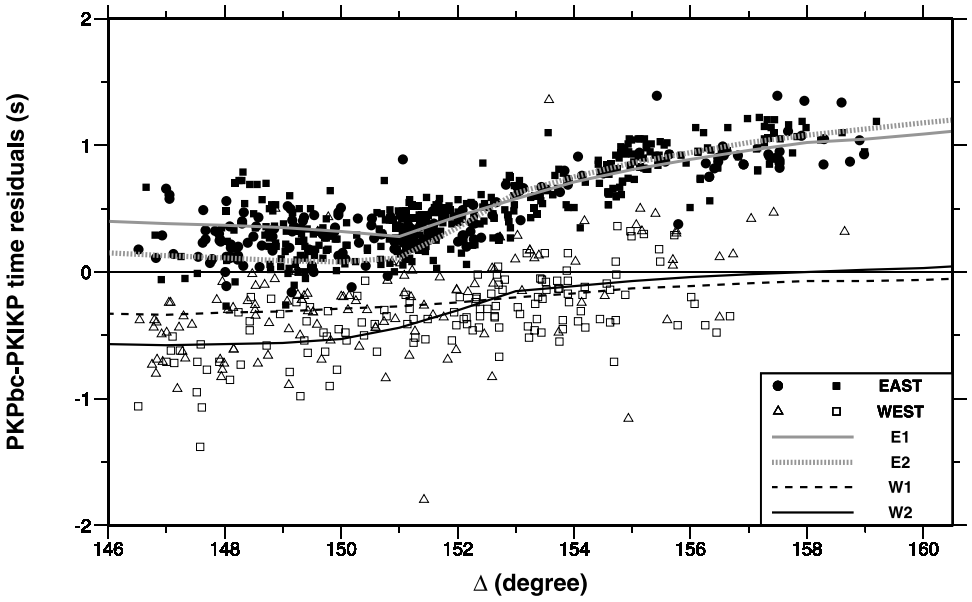

Figure 4. Observed *PKPbc-PKIKP* differential traveltime residuals with respect to PREM as a function of epicentral distance (Δ), along with predictions based on E1, E2, W1, and W2 (see Figure 6a for the velocity structures). The meaning of the symbols and lines is shown in the inset. Black solid circles and black solid squares represent the differential traveltime residuals for the *PKIKP* phases sampling the eastern hemisphere recorded in the GSN and the regional seismic networks (GRF, GRSN, GEOFON), respectively. Open triangles and open squares represent the differential traveltime residuals for the *PKIKP* phases sampling the western hemisphere recorded in the GSN and the regional seismic networks (BLSP, BANJO, SEDA, FREESIA), respectively. Distance corrections are made so that the differential traveltime residuals are plotted at the distances equivalent to a source depth of 200 km. Accordingly, the predicted differential traveltime residuals are made based on a source depth of 200 km.

(larger) bifurcation distance would indicate a larger (smaller) magnitude of the *P* velocity increase across the ICB. The radial velocity gradient of the inner core can be derived from fitting the subsequent move outs of the *PKiKP-PKIKP* phases [*Wen and Niu*, 2002]. The velocity models E1 and W1 that are appropriate for explaining the observed *PKiKP-PKIKP* waveforms are derived by [*Wen and Niu*, 2002] (E1 for the eastern hemisphere and W1 for the western hemisphere). However, there is a trade-off between the seismic velocity structure in the bottom of the outer core and the seismic velocity structure in the top of the inner core in explaining the *PKiKP-PKIKP* waveforms (Figures 3b and 3d) [*Wen and Niu*, 2002]. For example, the synthetic waveforms produced by models E1, E2 (black solid and black dashed traces in Figure 3b; velocity structures of E1, E2 in Figure 6a) and W1, W2 (black solid and black dashed traces in Figure 3d; velocity structures of W1, W2 in Figure 6a) are indistinguishable (E1 and W1 have PREM velocity structure in the bottom of the outer core; E2 and W2 have a low-velocity structure OW in the bottom of the outer core. We will discuss OW later in this paper). However, because the trade-off exists in such a way that a smaller velocity gradient in the bottom of the outer core requires a lower velocity structure in the top of the inner core, these velocity structures can be distinguished by the joint modeling of the *PKiKP-PKIKP* waveforms and the *PKPbc-PKIKP* differential traveltimes in the distance range of 146°–148°. In the distance range of 146°–148°, the *PKPbc* wave turns 400–240 km above the ICB, whereas the *PKIKP* wave propagates through the bottom of the outer core and the top 140–180 km of the inner core. A smaller velocity gradient in the bottom of the outer core and its coupled lower velocity structure in the top of the inner core would delay the *PKIKP* traveltimes more and produce smaller differential *PKPbc-PKIKP* traveltimes, and are thus distinguishable by the joint modeling of the differential *PKPbc-PKIKP* traveltimes. In our earlier study, we have resolved the coupled outer core–inner core velocity structures for the two hemispheres, which best explain the *PKiKP-PKIKP* waveforms and the *PKPbc-PKIKP* differential traveltime residuals for the seismic data sampling the two hemispheres [*Yu et al.*, 2005]. The eastern hemisphere has PREM velocity structure (a velocity gradient of 0.057 (km/s)/100 km) in the bottom of the outer core, a *P* velocity increase of 0.748 km/s across the ICB, and a coupled small velocity gradient of 0.0042 (km/s)/100 km in the top of the inner core (E1); the western hemisphere has a low-velocity structure OW (a velocity gradient of 0.041 (km/s)/100 km) in the bottom of the outer core, a *P* velocity increase of 0.645 km/s across the ICB, and a coupled steep velocity gradient of 0.049 (km/s)/100 km in the top of the inner core (W2) (Figure 6a). OW has reduced velocities relative to PREM linearly decreasing from 0% at 200 km above the ICB to −0.35% at the ICB (Figure 6a and Figure 6 of *Yu et al.* [2005]).

[11] With the velocity structures in the bottom of the outer core and the top of the inner core constrained by the joint modeling of the *PKiKP-PKIKP* waveforms and the *PKPbc-PKIKP* differential traveltime residuals at the distance range of 146°–148°, seismic velocity structures in the deeper part

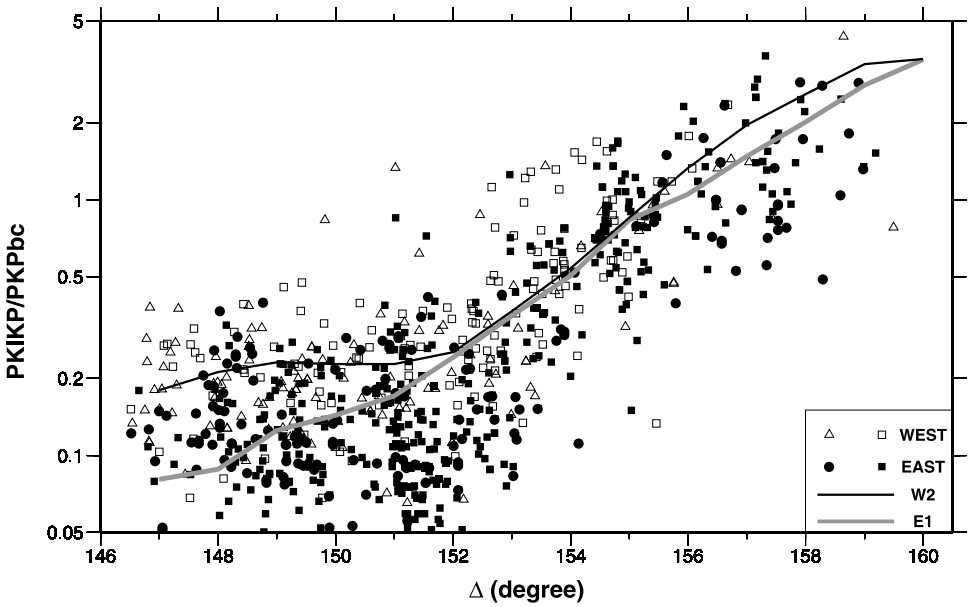

Figure 5. Observed *PKIKP*/*PKPbc* amplitude ratios as a function of epicentral distance (Δ) on a semilog scale, along with predicted amplitude ratios by W2 and E1 (see Figure 6 for the velocity and attenuation structures) based on a source depth of 200 km. The meaning of the symbols and lines is shown in the inset. Black solid circles and black solid squares represent the amplitude ratios for the *PKIKP* phases sampling eastern hemisphere recorded in the GSN and the regional seismic networks (GRF, GRSN, GEOFON), respectively. Open triangles and open squares represent the amplitude ratios for the *PKIKP* phases sampling the western hemisphere recorded in the GSN and the regional seismic networks (BLSP, BANJO, SEDA, FREESIA), respectively. Distance corrections are made so that the amplitude ratios are plotted at the distances equivalent to a source depth of 200 km. Predicted amplitude ratios are obtained from handpicking the maximum amplitudes of the *PKIKP* and *PKPbc* phases of the synthetic waveforms, calculated using the generalized ray theory [*Helmberger*, 1983].

of the inner core are derived from fitting the observed *PKPbc-PKIKP* differential traveltime residuals at distances greater than 148°. In what follows, we discuss velocity models and model resolution for the two hemispheres of the inner core on the basis of modeling the *PKPbc-PKIKP* differential time residuals.

[12] For the eastern hemisphere, the anomalously small velocity gradient in the top of the inner core is well resolved by the observed *PKiKP-PKIKP* move outs and the *PKPbc-PKIKP* differential time residuals. *Wen and Niu* [2002] have discussed in detail how the anomalous radial velocity gradient in the top 80 km of the inner core beneath the eastern hemisphere is resolved by the *PKiKP-PKIKP* waveform data. Readers are referred to *Wen and Niu* [2002] for the detailed discussions. The *PKPbc-PKIKP* data in this study confirm the existence of such an anomalous radial gradient in the top part of the eastern hemisphere. Models with a larger radial velocity gradient would also produce unacceptable misfits to the observed *PKPbc-PKIKP* time residuals at the distance range of 146°–156° (see an example in Figure 7a).

[13] The *PKPbc-PKIKP* time residuals further suggest that the anomalously small velocity gradient in the eastern hemisphere extends deeper than 80 km of the inner core. The extending depth of the small velocity gradient is in the range of 220–250 km, constrained by the observed change of trend in *PKPbc-PKIKP* time residuals at the distance of about 151°. Models with a shallower or a deeper extending depth would produce misfits to the differential time residuals. For example, an extending depth of 200 km would predict a change of differential time residual at a distance around 149° (Figure 7b), while an extending depth of 260 km would predict a change of differential time residual at a distance around 152° (Figure 7c). The extending depth of the anomalously small velocity gradient is constrained to be between 220 and 250 km.

[14] The increase and change of trend in the *PKPbc-PKIKP* time residuals at distances greater than 151° are used to constrain the nature of velocity transition (e.g., a first-order discontinuity or a steep transition in velocity) and the velocity structure in the deeper part of the inner core. A first-order velocity discontinuity at 235 km would predict a kink in differential *PKPbc-PKIKP* time residual at the distances around 151°–152° (gray solid line in Figure 7d; gray solid line in Figure 8). Such a kink is not observed either in the global data set (gray solid line, Figure 7d) or in the data recorded in the regional seismic networks for two events (see two examples in Figure 8). If we lower the velocity increase of the discontinuity and place the discontinuity at a slightly larger depth to fit the *PKPbc-PKIKP* time residuals at the distances of 151°–152°, the predicted differential time residuals would still produce a kink and misfit the *PKPbc-PKIKP* time residuals at larger distances for both the global data set (gray solid line, Figure 7e) and the data recorded in the regional seismic networks for two events (black solid line, Figure 8). A velocity model, which has a steeper transition (a velocity gradient of 0.1 (km/s)/

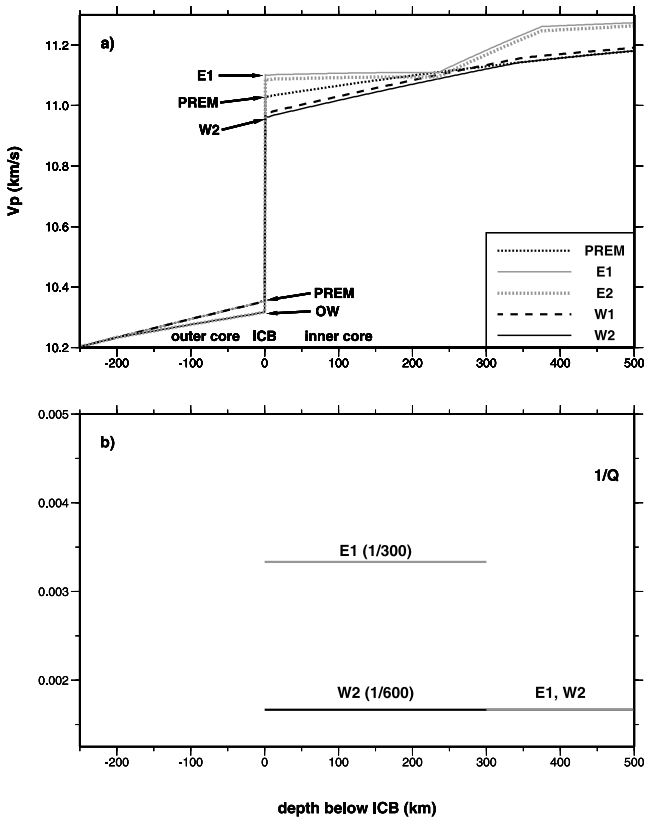

Figure 6. (a) Velocity and (b) attenuation structures in the bottom of the outer core and in the top 500 km of the inner core. The meaning of the lines in Figure 6a is shown in the inset. E1, W1 have PREM velocity structure in the bottom of the outer core; E2, W2 have a low-velocity structure OW in the bottom of the outer core. OW has reduced velocities relative to PREM linearly decreasing from 0% at 200 km above the ICB to −0.35% at the ICB [*Yu et al.*, 2005]. E1 and W2 are the best fitting models for the eastern and western hemispheres, respectively. The velocity models shown here are used to compute the synthetic *PKiKP-PKIKP* waveforms in Figure 3 and the synthetic *PKPbc-PKIKP* waveforms in Figure 11.

100 km) extending from 235 km to 375 km of the inner core (Figure 6a), can best explain the *PKPbc-PKIKP* differential time residuals at the distance range of 151°–154° for both the global data set (gray solid line in Figure 4; gray dashed line in Figure 7) and the data recorded in the regional seismic networks (gray dashed line, Figure 8).

[15] The *PKPbc-PKIKP* time residuals observed at distances greater than 155° suggest that a change of velocity gradient is needed following the steeper transition at a depth about 375 km below the ICB. A velocity model with a steeper transition extending larger than 400 km would predict differential traveltime residuals larger than the observations at greater distances (gray solid line, Figure 7f). A velocity gradient of 0.01 (km/s)/100 km, similar to the PREM gradient, at depths larger than 375 km below the ICB (gray solid line, Figure 6a) best predicts the observed differential traveltime residuals (gray solid line in Figure 4; gray dashed line in Figure 7). A velocity gradient smaller than the PREM gradient following the steeper transition would produce slight misfits to the observations at the distance range of 157°–159° (gray solid line, Figure 7g).

[16] Our modeling results suggest that the velocity structure for the eastern hemisphere has PREM velocity structure in the bottom of the outer core (a velocity gradient of 0.057 (km/s)/100 km), a velocity increase of 0.748 km/s across the ICB, an anomalously small velocity gradient of 0.0042 (km/s)/100 km extending to 235 km, followed by a steeper velocity gradient of 0.1 (km/s)/100 km extending from 235 km to 375 km, and a velocity gradient of 0.01 (km/s)/100 km extending from 375 km to the deeper portion of the inner core (E1, gray solid line in Figure 6a).

[17] For the western hemisphere, the observed *PKPbc-PKIKP* time residuals can be well explained by a simple velocity model W2 at the distance range of 146°–155° (open symbols, Figure 4). Because of the sparse data available at distances beyond 156°, we cannot resolve the velocity structure at depths larger than 375 km of the inner core. The velocity structure for the western hemisphere has an OW velocity structure in the bottom of the outer core (a velocity gradient of 0.041 (km/s)/100 km), a velocity increase of 0.645 km/s across the ICB, a steep velocity gradient of 0.049 (km/s)/100 km in the top 375 km, and an assumed PREM velocity at depths larger than 375 km of the inner core (W2, black solid line in Figure 6a).

3.3. Seismic Attenuation Structures in the Top 400 km of the Inner Core Along Equatorial Paths for the Two Hemispheres

[18] Seismic attenuation structures of the inner core are derived from joint fitting the observed *PKIKP*/*PKiKP* and *PKIKP*/*PKPbc* amplitude ratios. Smaller amplitude ratios would indicate smaller *PKIKP* amplitudes, and thus higher attenuation in the part of the inner core they sample. Attenuation is usually represented by quality factor Q, which is defined as the fractional loss of energy per cycle of wave oscillation as seismic waves travel through the medium. *Wen and Niu* [2002] have studied the attenuation structures in the top 80 km of the inner core along equatorial paths with an average Q value of 250 in the eastern hemisphere and an average Q value of 600 in the western hemisphere. In this study, we adopt Q models that are as simple as possible. The observed *PKIKP*/*PKiKP* amplitude ratios at the distance range of 131°–141° and the *PKIKP*/*PKPbc* amplitude ratios at the distance range of 146°–151° are consistently smaller for the data sampling the eastern hemisphere than those for the data sampling the western hemisphere; and the *PKIKP*/*PKPbc* data become indistinguishable for the two hemispheres at distances greater than 151°. For the eastern hemisphere, it is apparent that a change of Q with depth is required based on the observed amplitude ratios for the *PKIKP*/*PKiKP* data in the distance range of 131°–141° and the *PKIKP*/*PKPbc* data at distances less than 151° versus the observed amplitude ratios for the *PKIKP*/*PKPbc* data at larger distances. We thus adopt a simple attenuation model with an average Q in the top part and another average Q in the deeper part of the inner core, and we emphasize on best fitting both the *PKIKP*/*PKiKP* and *PKIKP*/*PKPbc* data sets (other than the *PKIKP*/*PKiKP* data alone as by *Wen and Niu* [2002]). For the western hemisphere, the seismic data show no evidence for a depth dependence of Q. We thus explore attenuation models with an

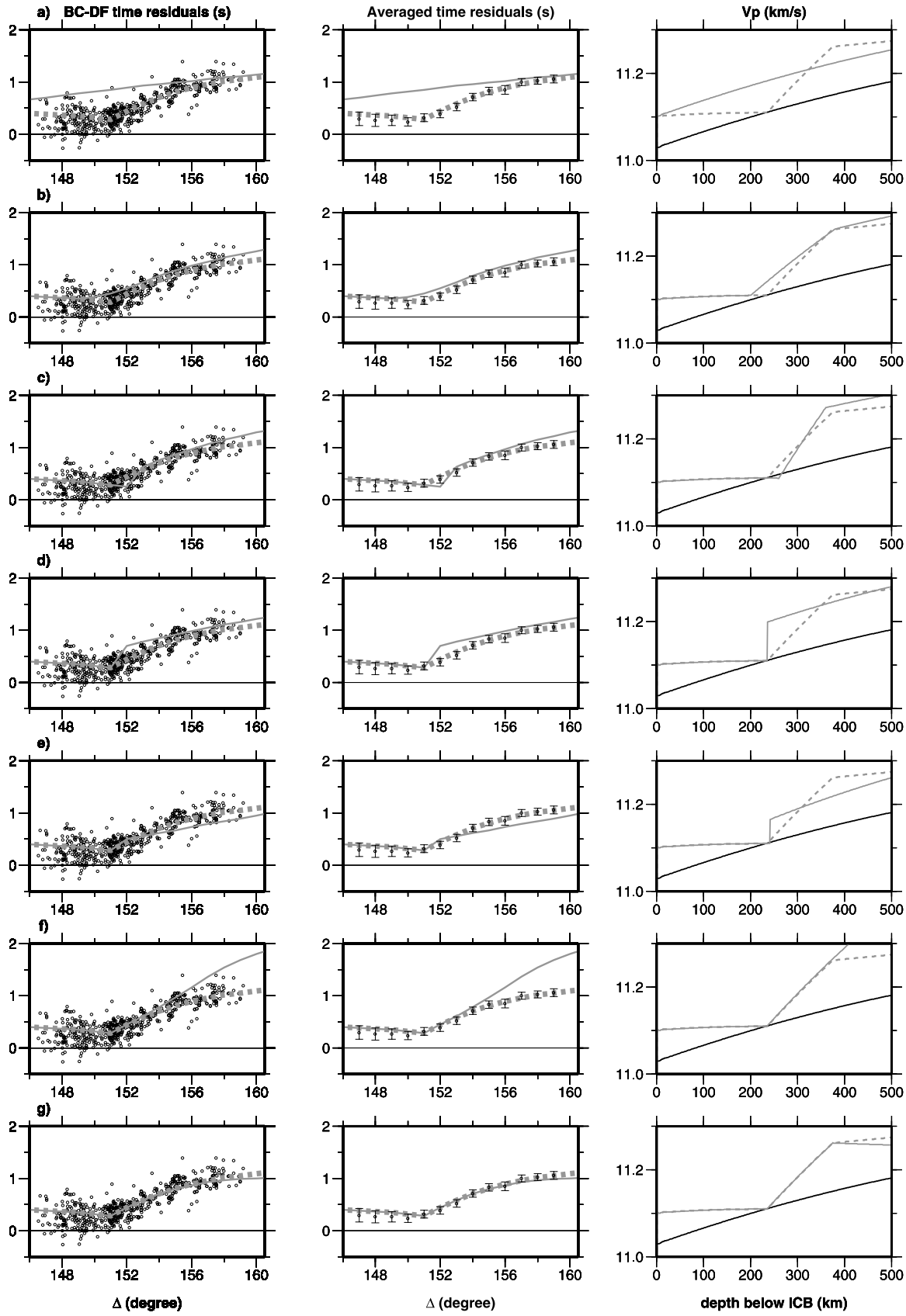
a) BC-DF time residuals (s)
Averaged time residuals (s)
Vp (km/s)
b)
c)
d)
e)
f)
g)
Δ (degree)
Δ (degree)
depth below ICB (km)

Figure 7

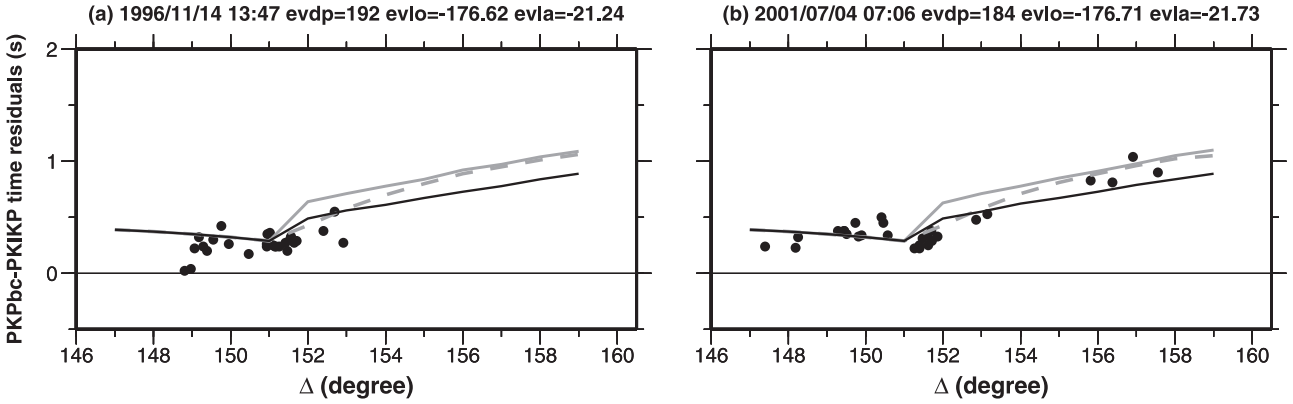

Figure 8. *PKPbc-PKIKP* differential traveltime residuals with respect to PREM as a function of epicentral distance (Δ) for the *PKIKP* phases sampling the eastern hemisphere recorded in the regional seismic networks of GRSN, GRF, GEOFON for two events, along with predictions based on the velocity model E1 (gray dashed line), a model with a velocity discontinuity at 235 km and a PREM velocity gradient in the deeper part of the inner core (gray solid line) (see gray solid line in Figure 7d (right) for such a velocity structure), and a model with a smaller magnitude of velocity discontinuity at 241 km below the ICB and a PREM velocity gradient in the deeper part of the inner core (black solid line) (see gray solid line in Figure 7e (right) for such a velocity structure). Event origin date, origin time, depth (evdp), longitude (evlo), and latitude (evla) are labeled in the top. Dense observations for these two events can exclude the model with a velocity discontinuity at depths of about 235–241 km below the ICB.

average Q in the top 400 km. Because the amplitude ratios are also sensitive to the velocity structures in the bottom of the outer core and the top of the inner core, our Q values in the inner core are inferred on the basis of the velocity models that best explain the *PKiKP-PKIKP* waveforms and the *PKPbc-PKIKP* differential traveltime residuals.

[19] For the eastern hemisphere, the observed amplitude ratios for the seismic data sampling the eastern hemisphere can be best explained by an attenuation structure with an average Q value of 300 in the top 300 km and an average Q value of 600 in the deeper part of the inner core (see Figure 5 for predictions of E1 and Figure 6b for the attenuation structure of E1). An average Q value of 300 can best explain the *PKIKP*/*PKiKP* amplitude ratios and the *PKIKP*/*PKPbc* amplitude ratios observed at the distance range of 146°–151°. A change of Q value from the top to the deeper part of the inner core beneath the eastern hemisphere is also well resolved by the seismic data. An average Q value of 300 in the top 400 km of the inner core (see gray dashed line labeled as E1_300 in Figures 9a and 9c for predictions) would underpredict the amplitude ratios at distances greater than 154°.

[20] For the western hemisphere, an average Q value of 600 in the top 400 km of the inner core can well explain the *PKIKP*/*PKiKP* and *PKIKP*/*PKPbc* amplitude ratios for the *PKIKP* phases sampling the western hemisphere (see Figure 5 for predictions of W2 and Figure 6b for the attenuation structure of W2).

[21] The above inferred hemispheric variation of attenuation structure is well resolved by the seismic data. For example, an average Q value of 600 in the top 400 km of the inner core, derived from fitting the amplitude ratios for the western hemisphere, would overpredict most of the *PKIKP*/*PKPbc* amplitude ratios at the distance range of 146°–160° for the *PKIKP* phases sampling the eastern hemisphere (see gray dotted line labeled as E1_600 in Figures 9a and 9c for predictions). An average Q value of 300 in the top 400 km of the inner core, on the other hand, would underpredict the *PKIKP* amplitudes at the distance range of 131°–141° [see *Wen and Niu*, 2002, Figure 5] and the *PKIKP*/*PKPbc* amplitude ratios at the distance range of 146°–160° (see black dotted line labeled as W2_300 in Figures 9b and 9d for predictions) for the seismic data sampling the western hemisphere.

Figure 7. (left) Observed *PKPbc*(*BC*)–*PKIKP*(*DF*) differential traveltime residuals for the *PKIKP* phases sampling the eastern hemisphere (open circles) with respect to PREM and (middle) their averages and standard deviations over each 1° as a function of epicentral distance (Δ), along with predicted differential traveltime residuals based on E1 (gray dashed lines) and some example models perturbed from E1 (gray solid lines). (right) Velocity profiles of PREM (black solid lines), E1 (gray dashed lines), and the perturbed models (gray solid lines) in the top 500 km of the inner core. The observed differential traveltime residuals are corrected and the predictions are made based on a source depth of 200 km. The perturbed models include those with (a) a PREM velocity gradient in the top 500 km of the inner core, (b) a small velocity gradient extending to 200 km below the ICB, (c) a small velocity gradient extending to 260 km below the ICB, (d) a small velocity gradient in the top 235 km, followed by a velocity discontinuity and a PREM velocity gradient in the deeper part of the inner core, (e) similar to Figure 7d but with a smaller magnitude of velocity increase at a depth of 241 km below the ICB, (f) a small velocity gradient in the top 235 km, followed by a steeper velocity transition extending deeper than 400 km below the ICB, and (g) a small velocity gradient in the top 235 km, followed by a steeper velocity transition extending from 235 km to 375 km and another small velocity gradient at depths larger than 375 km below the ICB.

[22] In explaining the *PKIKP*/*PKPbc* amplitude ratios at the *PKPbc* diffracted distances ($\Delta > 153^\circ$), there exists a trade-off between the velocity structure in the bottom of the outer core and the attenuation structure in the deeper part of the inner core. A higher velocity gradient in the bottom of the outer core (for example, PREM) would predict a smaller diffracted *PKPbc* amplitude and thus a larger *PKIKP*/*PKPbc* amplitude ratio. The *PKIKP*/*PKPbc* amplitude ratios observed at the *PKPbc* diffracted distances seem to support the inference of the low velocity gradient OW in the bottom of the outer core. Predictions of W1, which has PREM velocity in the bottom of the outer core and an average Q value of 600 in the top 400 km of the inner core (Figures 6a and 6b), would produce larger amplitude ratios than the observations at distances greater than 153° (see gray dashed line labeled as W1 in Figures 9b and 9d for predictions). An attenuation structure with low attenuation (an average Q value of 600) in the top 250 km and high attenuation (an average Q value of 300) in the deeper portion of the inner core is needed to explain the observed *PKIKP*/*PKPbc* amplitude ratios in the western hemisphere (see gray dotted line labeled as W11 in Figures 9b and 9d for predictions). It is unclear that such an attenuation model is physically plausible.

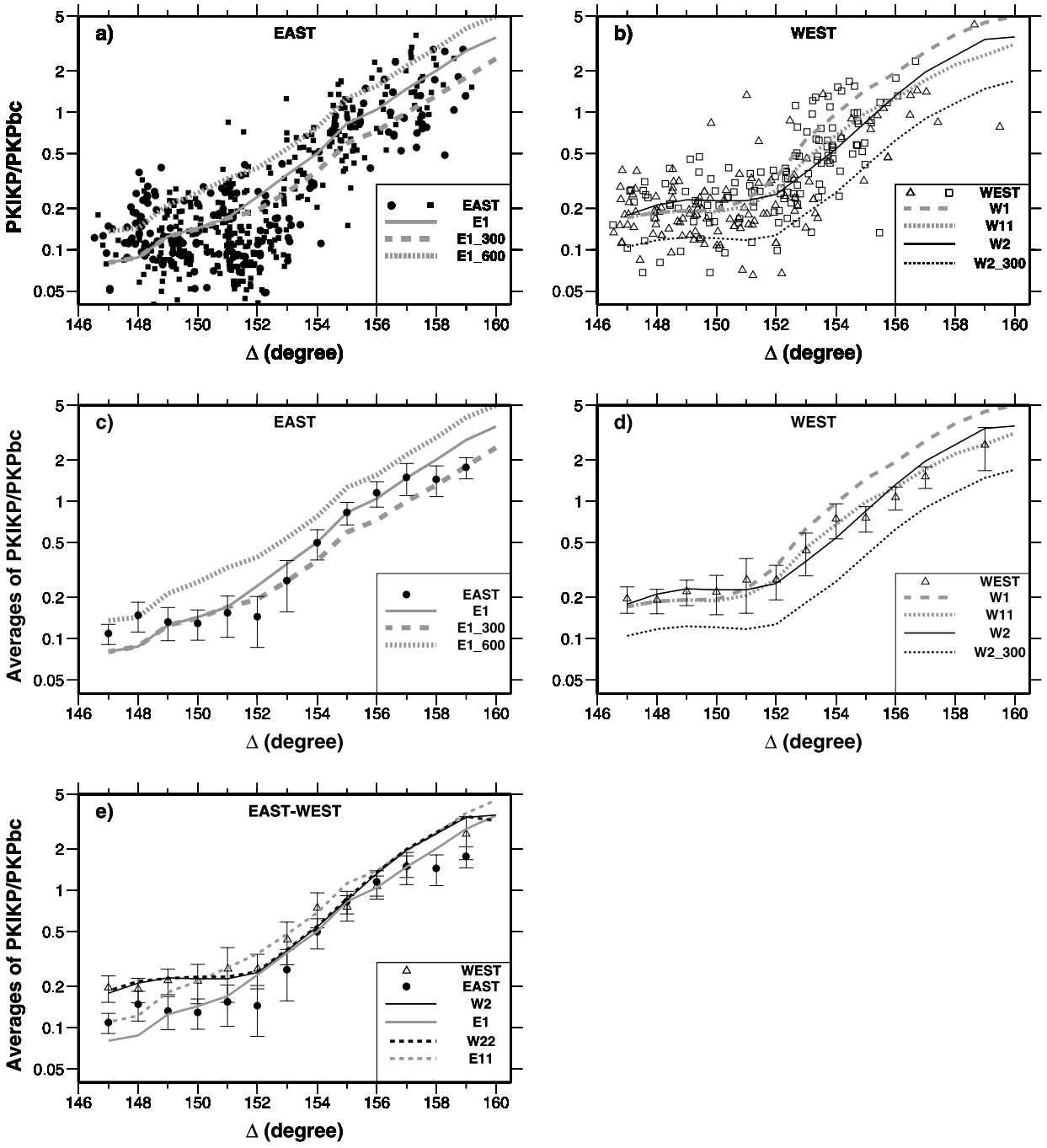

Figure 9

[23] *Cao and Romanowicz* [2004a] recently studied the hemispheric attenuation structure in the top 110 km of the inner core, based on the analyses of the amplitude ratios and differential traveltimes of the *PKiKP-PKIKP* phases observed at the distance range of 135°–144°. Their results confirmed the hemispheric pattern in attenuation structure in the top portion of the inner core reported earlier by *Wen and Niu* [2002]. However, they obtained different Q structures for the two hemispheres. They suggested that the eastern hemisphere has Q values increasing from 100 to 200 in the depth range of 32 km to 85 km of the inner core; the western hemisphere has Q values decreasing from 500 to 200 in the depth range of 32 km to 85 km of the inner core; and the hemispheric variation of attenuation disappears at depths of 85 km below the inner core boundary [*Cao and Romanowicz*, 2004a, Figures 5 and 7]. Complex Q values in the top 85 km in their attenuation models were inferred from the observed distance-varying *PKIKP* amplitudes. However, in practice, the *PKIKP* amplitudes observed at the distance range of 130°–140° do not have resolution to distinguish a model with a gradational change in Q value from a constant Q model in the top 85 km of the inner core. For example, synthetic *PKIKP* amplitudes based on their attenuation model for the western hemisphere (WCR, gray dashed traces in Figure 3d) cannot be distinguished from a model with a constant Q value of 600 (W2, black dashed traces in Figure 3d) on the basis of fitting the observations (Figure 3c). For the eastern hemisphere, their Q values would predict smaller *PKIKP* amplitudes (ECR, gray dashed traces in Figure 3b) than the observations (Figure 3a) at distances greater than 135°. A modified attenuation model E11 with increased Q values from 200 to 400 in the depth range of 32 km to 85 km of the inner core (E11, gray solid traces in Figure 3b) would explain the *PKIKP* amplitudes for those sampling the eastern hemisphere (Figure 3a). Such a modified model (E11, gray solid traces in Figure 3b) cannot be distinguished from a model with a constant Q value of 300 (E1, black solid traces in Figure 3b) on the basis of fitting the observed *PKIKP* waveforms sampling the eastern hemisphere (Figure 3a). We thus adopt simple attenuation models in the top part of the inner core for the two hemispheres. To understand whether the inferred hemispheric difference in attenuation is confined in the top 85 km of the inner core, we test models with uniform Q value at depths larger than 85 km of the inner core and compare their predicted *PKIKP*/*PKPbc* amplitude ratios with the observations. Predictions from their attenuation model for the western hemisphere in the top 85 km followed by a Q value of 600 in the deeper portion of the inner core (model W22, see black dashed line labeled as W22 in Figure 9e for predictions) are indistinguishable from those of W2 (black solid line labeled as W2 in Figure 9e) and can fit the *PKIKP*/*PKPbc* amplitude ratios equally well. However, a model with the modified attenuation structure in the top 85 km to fit the *PKIKP* waveforms for the eastern hemisphere (E11) and a uniform Q value of 600 in the deeper portion of the inner core (see gray dashed line labeled as E11 in Figure 9e for predictions) would predict larger *PKIKP*/*PKPbc* amplitude ratios than the observations at distances larger than 149° for the *PKIKP* phases sampling the eastern hemisphere, indicating that the low Q value inferred for the top part of the eastern hemisphere must extend to the depths larger than 85 km of the inner core. We thus conclude that the hemispheric attenuation structure within the top 85 km of the inner core is not sufficient to explain the observed *PKIKP*/*PKPbc* amplitude ratios and that the hemispheric attenuation must extend deeper than 85 km below the inner core boundary.

[24] In summary, the seismic data suggest that the east-west hemispheric variations in velocity extend deeper than 375 km of the inner core along equatorial paths. The velocity and attenuation structures in the western hemisphere are relatively simple, while those in the eastern hemisphere are complex. The western hemisphere has a steep velocity gradient, low velocity, and low attenuation (an average Q value of 600) in the top 375 km. The eastern hemisphere has an anomalously small velocity gradient, high velocity and high attenuation (an average Q value of 300) in the top 235 km, a velocity gradient similar to the PREM gradient and low attenuation (an average Q value of 600) at depths larger than 375 km, and a steeper velocity transition between. The top 235 km of the inner core beneath the eastern hemisphere is anomalous compared to the rest of the inner core in having a small velocity gradient, high velocity and high attenuation.

3.4. Waveform Modeling

[25] Modeling the *PKiKP-PKIKP* waveforms has been proved to be extremely useful to constrain the detailed seismic structures in the top of the inner core [*Wen and*

Figure 9. Observed *PKIKP*/*PKPbc* amplitude ratios plotted at the distances equivalent to a source depth of 200 km (Figures 9a and 9b) and (Figures 9c, 9d, and 9e) their averages and standard deviations over each 1° as a function of epicentral distance (Δ) on a semilog scale, along with predicted amplitude ratios for several models for a source depth of 200 km. The meaning of the symbols and lines is shown in the inset. Predicted amplitude ratios are based on several coupled velocity and attenuation models: (a, c) E1 (see the velocity structure in Figure 6a and the attenuation structure in Figure 6b); E1_300 which has a velocity structure of E1 but with an average Q value of 300 in the top 400 km of the inner core; E1_600 which has a velocity structure of E1 but with an average Q value of 600 in the top 400 km of the inner core; (b, d) W1 which has a velocity structure of W1 and an average Q value of 600 in the top 400 km of the inner core; W11 which has a velocity structure of W1 but with an average Q value of 600 in the top 250 km and an average Q value of 300 in the deeper part of the inner core; W2 (see the velocity structure in Figure 6a and the attenuation structure in Figure 6b); W2_300 which has a velocity structure of W2 but with an average Q value of 300 in the top 400 km of the inner core; (e) W22 which has a velocity structure of W2 but with decreased Q values from 500 to 200 in the depth range of 32 km to 85 km and a Q value of 600 in the deeper portion of the inner core; E11 which has a velocity structure of E1 but with increased Q values from 200 to 400 in the depth range of 32 km to 85 km and a Q value of 600 in the deeper portion of the inner core.

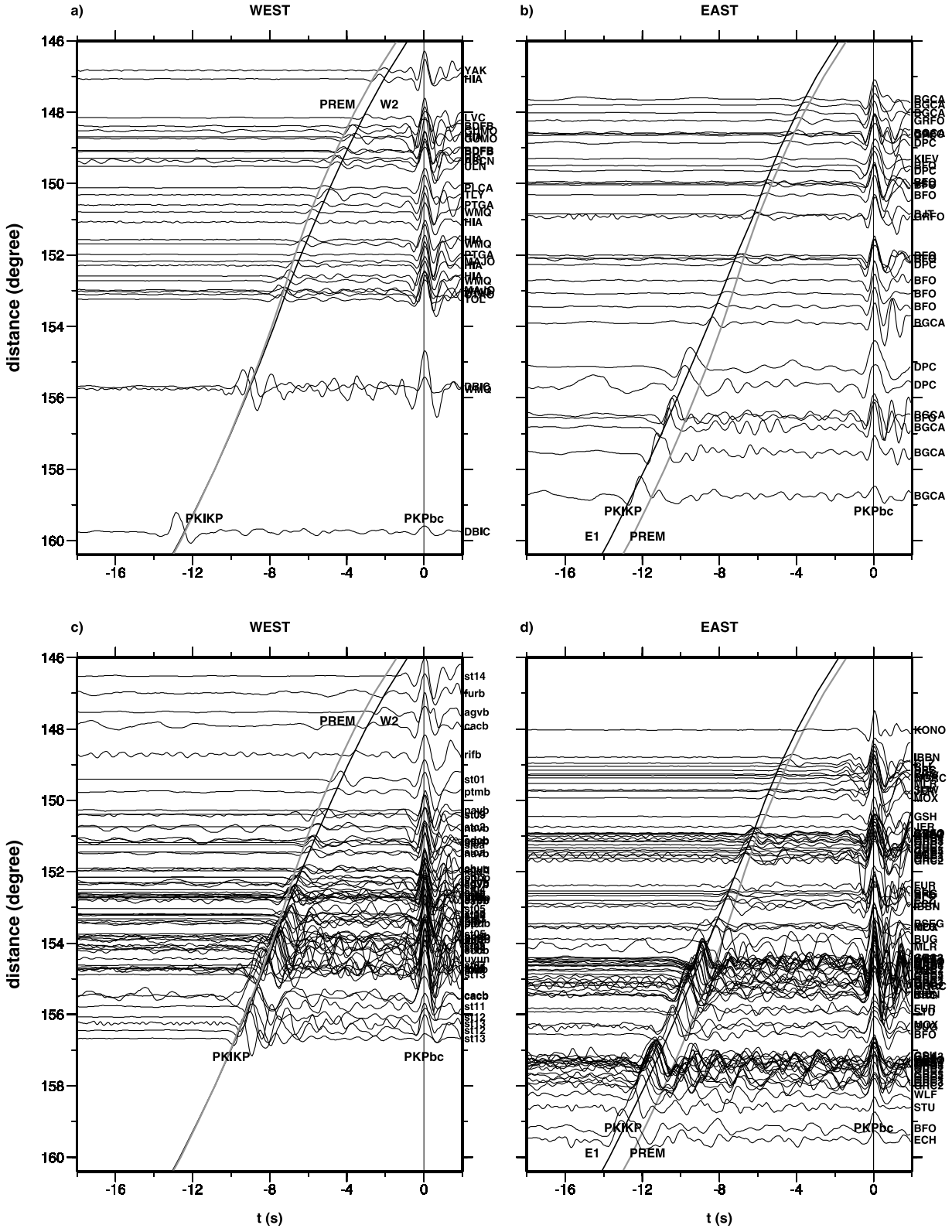
a)
WEST
b)
EAST
c)
WEST
d)
EAST
distance (degree)
t (s)
PREM
W2
PKIKP
PKPbc
E1
YAK
HIA
PLCA
TLY
PTGA
WMQ
DBIC
BGCA
DPC
BFO
GRFO
KIEV
KONO
MOX
GSH
EUR
BUG
WLR
WLF
STU
ECH
st14
furb
agvb
cacb
rifb
st01
ptmb
st11
st12
st13
146
148
150
152
154
156
158
160
-16
-12
-8
-4
0

Figure 10

Niu, 2002]. In this study, we further compare the observed seismograms with the synthetics predicted based on the velocity and attenuation models derived from fitting the differential traveltimes and amplitudes ratios of the *PKPbc-PKIKP* phases. Synthetic waveforms are calculated using the generalized ray theory method [*Helmberger*, 1983]. In the synthetic calculations, the velocity models in the outer core are divided into 227 layers, with a thickness of 10 km for most of the layers. The velocity models in the inner core are divided into 418 layers, which have a thickness of 2 km in the top 370 layers and a thickness of 10 km in the lower 48 layers in the inner core. The synthetic *PKiKP-PKIKP* and *PKPbc-PKIKP* waveforms based on the seismic velocity and attenuation models E1 and W2 match well the observed waveforms for the two hemispheres (Figures 3, 10, and 11).

4. Mantle Effects

[26] It is essential to understand how the differential traveltimes and amplitude ratios of these core phases would be affected by the seismic heterogeneities elsewhere, especially those near the core-mantle boundary (CMB). The Fresnel zone is about 150 km at the CMB for the *PKP* waves we use with a dominant frequency of 1 Hz. For the *PKiKP-PKIKP* phases, the two rays are separated by about 50 km at the CMB, and the Fresnel zones of these two phases overlap [see, e.g., *Niu and Wen*, 2001, Figure 4]. In addition, different waveform characteristics are observed for some regions of the CMB sampled by the *PKIKP* phases bottoming different hemispheres of the inner core recorded by the dense seismic arrays [*Niu and Wen*, 2001]; and same waveform characteristics are observed for different regions of the CMB that the *PKIKP* phases sample the same hemisphere of the inner core recorded by the dense seismic arrays (Figure 3 and Figures 3 and 5 of *Wen and Niu* [2002]). So, the *PKiKP-PKIKP* observations are affected little by the seismic heterogeneities near the CMB. For the *PKPbc-PKIKP* phases, the separations of the two rays are about 300 km at the CMB, about double the size of the Fresnel zone. It is difficult to correct for the mantle effects, as such small-scale seismic heterogeneities are not well known. However, it would be inconceivable that small-scale seismic heterogeneities in the mantle would preferentially affect one branch of these core phase pairs in a hemispheric scale. Dense observations would indeed allow us to exclude the possibility that the signals observed in the *PKPbc-PKIKP* data are originated from the CMB. In the regions sampled by dense observations, the Fresnel zones of the *PKIKP* and *PKPbc* phases overlap at the CMB (see an example in Figure 12). The CMB structures would affect the *PKIKP* and *PKPbc* phases in the same way, and thus cannot provide an explanation for the observed *PKPbc-PKIKP* phases.

5. Possible Interpretations

[27] It has been suggested that the variations in velocity, attenuation, and the correlation of high (low) velocity with high (low) attenuation may be explained by different alignments of the hexagonal close packed (hcp) iron crystals, under the hypothesis that the axis of high (low) velocity of the hcp iron crystal corresponds to that of high (low) attenuation [*Yu and Wen*, 2006]. Such a mechanism, while it may readily explain the velocity and attenuation structures in the western hemisphere, would require the hcp iron crystals are aligned in such a way that the alignment would cancel the pressure effect such that the seismic velocity does not increase with depth in the top 235 km of the eastern hemisphere. A change of velocity and attenuation structures in the depth range of 235–375 km would also require the alignment of the hcp iron crystals in the deeper portion of the inner core to be different from that in the top. It is possible that other factors, such as partial melt, also play an important role in generating the anomalous top layer in the eastern hemisphere [*Wen and Niu*, 2002].

6. Conclusions

[28] We have analyzed 260 *PKiKP-PKIKP* and 830 *PKPbc-PKIKP* phases recorded in the Global Seismographic Network from 1990 to 2001 and in several regional seismographic networks to study seismic velocity and attenuation structures in the top 400 km of the Earth's inner core along equatorial paths. The seismic observations of the *PKiKP-PKIKP* and *PKPbc-PKIKP* phases exhibit distinctive "east-west" hemispheric patterns:

[29] 1. At the distance ranges of 131°–141° and 146°–151°, *PKIKP* phases arrive about 0.3 s earlier than the theoretical arrivals based on PREM for the *PKIKP* phases sampling the "eastern hemisphere" (40°E–180°E) and about 0.4 s later for those sampling the "western hemisphere" (180°W–40°E). At distances greater than 151°, *PKIKP* phases arrive about 0.7 s earlier than the predicted arrivals based on PREM for those sampling the eastern hemisphere and about 0.1 s later for those sampling the western hemisphere.

[30] 2. Amplitude ratios of the *PKIKP*/*PKiKP* phases observed at the distance range of 131°–141° and of the

Figure 10. Example waveforms for the *PKIKP* and *PKPbc* phases sampling the (a, c) western and (b, d) eastern hemispheres, along with *PKIKP* theoretical arrivals based on PREM (gray lines), W2 (black lines) (Figures 10a and 10c), and E1 (black lines) (Figures 10b and 10d). Observed waveforms are selected from the recordings in the GSN (Figures 10a and 10b), the regional networks BLSP, BANJO, SEDA in South America (Figure 10c), and GRF, GRSN, GEOFON, MEDNET, GEOSCOPE, GSN, CRSN in Europe for three events: origin time 14 November 1996, 1347:38 UT, 12 April 1997, 0921:56 UT, and 14 June 2000, 0215:26 UT (Figure 10d). Waveforms are aligned according to the maximum amplitudes of the *PKPbc* phases. Waveforms are normalized according to the maximum amplitudes of the *PKPbc* phases before the diffracted distances and of the *PKIKP* phases beyond the *PKPbc* diffracted distances. Distance corrections are made such that each trace is aligned at the distance equivalent to a source depth of 200 km. The predicted *PKIKP* arrivals are based on a source depth of 200 km. Seismic waveforms exhibit same characteristics for those recorded in the GSN and those recorded in the regional seismic networks for the *PKIKP* phases sampling the two hemispheres.

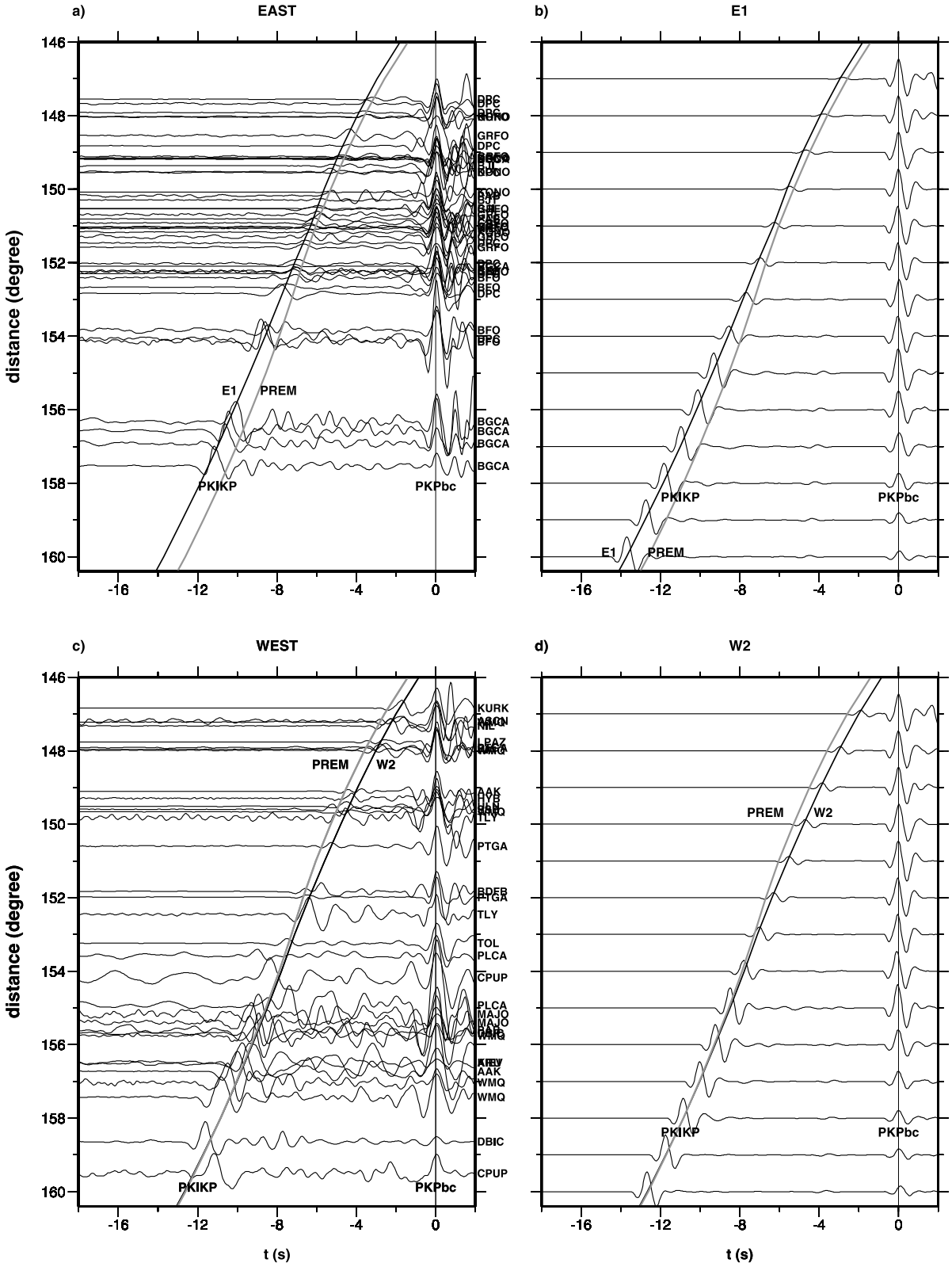

Figure 11. Observed waveforms of the *PKIKP* and *PKPbc* phases sampling the (a) eastern and (c) western hemispheres, selected from the recordings in the GSN; synthetic waveforms calculated based on velocity and attenuation models (b) E1 and (d) W2 (see Figure 6 for the velocity and attenuation structures). The predicted *PKIKP* arrivals based on E1 (black lines) (Figures 11a and 11b), W2 (black lines) (Figures 11c and 11d), and PREM (gray lines) (Figures 11a, 11b, 11c, and 11d) are also plotted. Waveforms are aligned and normalized in the same way as those in Figure 10. Distance corrections, *PKIKP* theoretical arrivals and synthetic waveforms are made based on a source depth of 200 km as those in Figure 10.

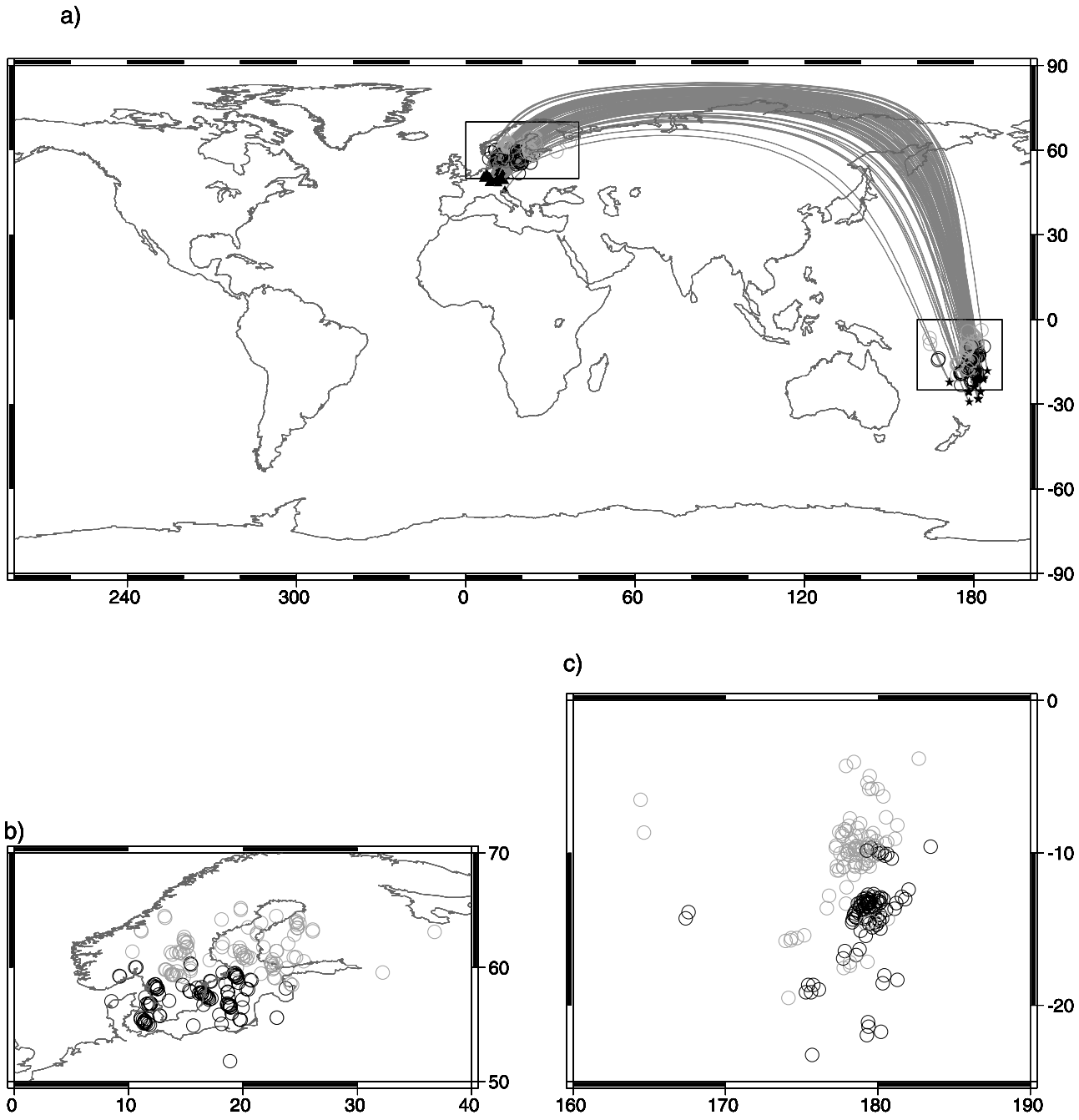

Figure 12. (a) Entry and exit points at the core-mantle boundary (CMB) for the *PKIKP* (black circles) and *PKPbc* (gray circles) phases for two example regions with dense observations, along with great circle paths (gray lines). (b, c) Blow-ups near the region of exit points (Figure 12b) and entry points (Figure 12c) at the CMB. Stars and triangles represent locations of earthquakes and seismic stations, respectively. The size of the circles is equivalent to the size of the Fresnel zones at the CMB for the *PKP* waves with a dominant frequency of 1 Hz. Note that the Fresnel zones of the *PKIKP* and *PKPbc* phases overlap in the regions sampled by dense observations.

PKIKP/*PKPbc* phases observed at the distance range of 146°–151° are, in general, smaller in the eastern hemisphere than in the western hemisphere. The observed *PKIKP*/*PKPbc* amplitude ratios become indistinguishable for the two hemispheres at distances greater than 151°. The above observations can be explained by two different types of seismic velocity and attenuation models along equatorial paths, one for each hemisphere, in the top 400 km of the inner core. The velocity structure for the eastern hemisphere has a velocity increase of 0.748 km/s across the ICB, a small velocity gradient of 0.0042 (km/s)/100 km in the top 235 km, followed by a steeper velocity gradient of 0.1 (km/s)/100 km extending from 235 km to 375 km, and a velocity gradient of 0.01 (km/s)/100 km in the deeper portion of the

inner core; the attenuation structure has an average Q value of 300 in the top 300 km and an average Q value of 600 in the deeper portion of the inner core. In contrast, the velocity and attenuation structures for the western hemisphere are relatively simple. The velocity structure has a velocity increase of 0.645 km/s across the ICB and a velocity gradient of 0.049 (km/s)/100 km in the top 375 km; the attenuation structure has an average Q value of 600 in the top 375 km of the inner core. Our seismic data suggest that the inner core hemispheric variations in velocity extend deeper than 375 km below the ICB and the top 235 km of the inner core in the eastern hemisphere is anomalous compared to the rest of the inner core in having a small velocity gradient, high velocity, and high attenuation.

[31] **Acknowledgments.** We are grateful to the IRIS-DMC, GSN, BANJO, SEDA, BLSP, GRF, GRSN, GEOFON, GEOSCOPE, MEDNET, CRSN, Kazakhstan, and FREESIA for the high-quality seismic data. We thank Fenglin Niu for sharing the data collections. Paul Richards, Associate Editor Michael Ritzwoller, and an anonymous reviewer provided valuable comments on the presentation of this manuscript. This work is supported by an NSF grant EAR 0207746.

References

Beghein, C., and J. Trampert (2003), Robust normal mode constraints on inner-core anisotropy from model space search, *Science*, *299*, 552–555.

Cao, A., and B. Romanowicz (2004a), Hemispherical transition of seismic attenuation at the top of the Earth's inner core, *Earth Planet. Sci. Lett.*, *228*, 243–253.

Cao, A., and B. Romanowicz (2004b), Constraints on density and shear velocity contrasts at the inner core boundary, *Geophys. J. Int.*, *157*, 1146–1151.

Cormier, V. F. (1981), Short-period *PKP* phases and the anelastic mechanism of the inner core, *Phys. Earth Planet. Inter.*, *24*, 291–301.

Cormier, V. F., and G. L. Choy (1986), A search for lateral heterogeneity in the inner core from differential travel times near *PKP-D* and *PKP-C*, *Geophys. Res. Lett.*, *13*, 1553–1556.

Cormier, V. F., and X. Li (2002), Frequency-dependent seismic attenuation in the inner core: 2. A scattering and fabric interpretation, *J. Geophys. Res.*, *107*(B12), 2362, doi:10.1029/2002JB001796.

Cormier, V. F., X. Xu, and G. L. Choy (1998), Seismic attenuation of the inner core: Viscoelastic or stratigraphic?, *Geophys. Res. Lett.*, *25*, 4019–4022.

Creager, K. C. (1992), Anisotropy of the inner core from differential travel times of the phases *PKP* and *PKIKP*, *Nature*, *356*, 309–314.

Creager, K. C. (1997), Inner core rotation rate from small-scale heterogeneity and time-varying travel times, *Science*, *278*, 1284–1288.

Creager, K. C. (1999), Large-scale variations in inner core anisotropy, *J. Geophys. Res.*, *104*, 23,127–23,139.

Cummins, P., and L. R. Johnson (1988), Synthetic seismograms for an inner core transition of finite thickness, *Geophys. J.*, *94*, 21–24.

Doornbos, D. J. (1974), The anelasticity of the inner core, *Geophys. J. R. Astron. Soc.*, *38*, 397–415.

Doornbos, D. J. (1983), Observable effects of the seismic absorption band in the Earth, *Geophys. J. R. Astron. Soc.*, *75*, 693–711.

Durek, J. J., and B. Romanowicz (1999), Inner-core anisotropy inferred by direct inversion of normal mode spectra, *Geophys. J. Int.*, *139*, 599–622.

Dziewonski, A., and D. L. Anderson (1981), Preliminary reference Earth model, *Phys. Earth Planet. Inter.*, *25*, 297–356.

Garcia, R. (2002), Constraints on upper inner-core structure from waveform inversion of core phases, *Geophys. J. Int.*, *150*, 651–664.

Garcia, R., and A. Souriau (2000), Inner core anisotropy and heterogeneity level, *Geophys. Res. Lett.*, *27*, 3121–3124.

Helmberger, D. V. (1983), Theory and application of synthetic seismograms, in *Earthquakes: Observation, Theory and Interpretation*, edited by H. Kanamori, pp. 173–222, Soc. Ital. di Fis., Bologna.

Ishii, M., and A. M. Dziewonski (2002), The innermost inner core of the Earth: Evidence for a change in anisotropic behavior at the radius of about 300 km, *Proc. Natl. Acad. Sci. U.S.A.*, *99*, 14,026–14,030.

Ishii, M., J. Tromp, A. M. Dziewonski, and G. Ekström (2002), Joint inversion of normal mode and body wave data for inner core anisotropy: 1. Laterally homogeneous anisotropy, *J. Geophys. Res.*, *107*(B12), 2379, doi:10.1029/2001JB000712.

Kaneshima, S. (1996), Mapping heterogeneity of the uppermost inner core using two pairs of core phases, *Geophys. Res. Lett.*, *23*, 3075–3078.

Koper, K. D., J. M. Franks, and M. Dombrovskaya (2004), Evidence for small-scale heterogeneity in Earth's inner core from a global study of PKiKP coda waves, *Earth Planet. Sci. Lett.*, *228*, 227–241.

Krasnoshchekov, D. N., P. B. Kaazik, and V. M. Ovtchinnikov (2005), Seismological evidence for mosaic structure of the surface of the Earth's inner core, *Nature*, *435*, 483–487.

Laske, G., and G. Masters (1999), Limits on differential rotation of the inner core from an analysis of the Earth's free oscillations, *Nature*, *402*, 66–69.

Li, A., and P. G. Richards (2003), Using earthquake doublets to study inner core rotation and seismicity catalog precision, *Geochem. Geophys. Geosyst.*, *4*(9), 1072, doi:10.1029/2002GC000379.

Li, X., and V. F. Cormier (2002), Frequency-dependent seismic attenuation in the inner core, 1. A viscoelastic interpretation, *J. Geophys. Res.*, *107*(B12), 2361, doi:10.1029/2002JB001795.

Masters, G., and F. Gilbert (1981), Structure of the inner core inferred from observations of its spheroidal shear modes, *Geophys. Res. Lett.*, *8*, 569–571.

McSweeney, T., K. C. Creager, and R. T. Merrill (1997), Depth extent of inner-core seismic anisotropy and implications for geomagnetism, *Phys. Earth Planet. Inter.*, *101*, 131–156.

Morelli, A., A. M. Dziewonski, and J. H. Woodhouse (1986), Anisotropy of the inner core inferred from *PKIKP* travel times, *Geophys. Res. Lett.*, *13*, 1545–1548.

Niu, F., and L. Wen (2001), Hemispherical variations in seismic velocity at the top of the Earth's inner-core, *Nature*, *410*, 1081–1084.

Niu, F., and L. Wen (2002), Seismic anisotropy in the top 400 km of the inner core beneath the "eastern" hemisphere, *Geophys. Res. Lett.*, *29*(12), 1611, doi:10.1029/2001GL014118.

Oreshin, S. I., and L. P. Vinnik (2004), Heterogeneity and anisotropy of seismic attenuation in the inner core, *Geophys. Res. Lett.*, *31*, L02613, doi:10.1029/2003GL018591.

Ouzounis, A., and K. C. Creager (2001), Isotropy overlying anisotropy at the top of the inner core, *Geophys. Res. Lett.*, *28*, 4331–4334.

Poupinet, G., R. Pillet, and A. Souriau (1983), Possible heterogeneity of the Earth's core deduced from *PKIKP* travel times, *Nature*, *305*, 204–206.

Shearer, P. M. (1994), Constraints on inner core anisotropy from *PKP* (*DF*) travel times, *J. Geophys. Res.*, *99*, 19,647–19,659.

Song, X. (1996), Anisotropy in central part of inner core, *J. Geophys. Res.*, *101*, 16,089–16,097.

Song, X. (2000), Joint inversion for inner core rotation, inner core anisotropy, and mantle heterogeneity, *J. Geophys. Res.*, *105*, 7931–7943.

Song, X., and D. V. Helmberger (1993), Anisotropy of the Earth's inner core, *Geophys. Res. Lett.*, *20*, 285–288.

Song, X., and D. V. Helmberger (1995a), Depth dependency of anisotropy of Earth's inner core, *J. Geophys. Res.*, *100*, 9805–9816.

Song, X., and D. V. Helmberger (1995b), A *P* wave velocity model of Earth's core, *J. Geophys. Res.*, *100*, 9817–9830.

Song, X., and D. V. Helmberger (1998), Seismic evidence for an inner core transition zone, *Science*, *282*, 924–927.

Song, X., and A. Li (2000), Support for differential inner core superrotation from earthquakes in Alaska recorded at South Pole station, *J. Geophys. Res.*, *105*, 623–630.

Song, X., and P. G. Richards (1996), Seismological evidence for differential rotation of the Earth's inner-core, *Nature*, *382*, 221–224.

Souriau, A., and B. Romanowicz (1996), Anisotropy in inner core attentuation: A new type of data to constrain the nature of the solid core, *Geophys. Res. Lett.*, *23*, 1–4.

Souriau, A., and B. Romanowicz (1997), Anisotropy in the inner core: Relation between *P*-velocity and attenuation, *Phys. Earth Planet. Inter.*, *101*, 33–47.

Souriau, A., and P. Roudil (1995), Attentuation in the uppermost inner core from broadband GEOSCOPE *PKP* data, *Geophys. J. Int.*, *123*, 572–587.

Souriau, A., and M. Souriau (1989), Ellipticity and density at the inner core boundary from subcritical *PKiKP* and *PcP* data, *Geophys. J. Int.*, *98*, 39–54.

Stroujkova, A., and V. F. Cormier (2004), Regional variations in the uppermost 100 km of the Earth's inner core, *J. Geophys. Res.*, *109*, B10307, doi:10.1029/2004JB002976.

Sun, X., and X. Song (2002), *PKP* travel times at near antipodal distances: Implications for inner core anisotropy and lowermost mantle structure, *Earth Planet. Sci. Lett.*, *195*, 429–445.

Tanaka, S., and H. Hamaguchi (1997), Degree one heterogeneity and hemispherical variation of anisotropy in the inner core from *PKP* (*BC*)-*PKP* (*DF*) times, *J. Geophys. Res.*, *102*, 2925–2938.

Tromp, J. (1993), Support for anisotropy of the Earth's inner core from free oscillations, *Nature*, *366*, 678–681.

Tromp, J. (1995), Normal-mode splitting observations from the great 1994 Bolivia and Kuril Islands earthquakes: Constraints on the structure of the mantle and inner core, *GSA Today*, *5*, 137–151.

Tseng, T.-L., B.-S. Huang, and B.-H. Chin (2001), Depth-dependent attenuation in the uppermost inner core from the Taiwan short period seismic array *PKP* data, *Geophys. Res. Lett.*, *28*, 459–462.

Vidale, J. E., and P. S. Earle (2000), Fine-scale heterogeneity in the Earth's inner core, *Nature*, *361*, 273–275.

Vinnik, L., B. Romanowiz, and L. Berger (1994), Anisotropy in the center of the inner core, *Geophys. Res. Lett.*, *21*, 1671–1674.

Wen, L., and F. Niu (2002), Seismic velocity and attenuation structures in the top of the Earth's inner core, *J. Geophys. Res.*, *107*(B11), 2273, doi:10.1029/2001JB000170.

Woodhouse, J. H., D. Giardini, and X.-D. Li (1986), Evidence for inner core anisotropy from free oscillations, *Geophys. Res. Lett.*, *13*, 1549–1552.

Yu, W., and L. Wen (2006), Inner core attenuation anisotropy, *Earth Planet. Sci. Lett.*, *245*, 581–594.

Yu, W., L. Wen, and F. Niu (2005), Seismic velocity structure in the Earth's outer core, *J. Geophys. Res.*, *110*, B02302, doi:10.1029/2003JB002928.

Zhang, J., X. Song, Y. Li, P. G. Richards, X. Sun, and F. Waldhauser (2005), Inner core differential motion confirmed by earthquake waveform doublets, *Science*, *309*, 1357–1360.

L. Wen and W. Yu, Department of Geosciences, State University of New York at Stony Brook, Stony Brook, NY 11794-2100, USA. (lianxing.wen@sunysb.edu; yu@mantle.geo.sunysb.edu)